Sliver Cells in Thermophotovoltaic Systems

Niraj Lal

A thesis submitted for the degree of
Bachelor of Science with Honours in Physics at
The Australian National University

May, 2007

Declaration

This thesis is an account of research undertaken between July 2006 and May 2007 at the Centre for Sustainable Energy Systems and the Department of Physics, The Australian National University, Canberra, Australia.

Except where acknowledged in the customary manner, the material presented in this thesis is, to the best of my knowledge, original and has not been submitted in whole or part for a degree in any university.

Niraj Lal
May, 2007

Acknowledgements

There are a number of many people without whom this thesis would not have been possible. First and foremost I would like to thank my supervisor Professor Andrew Blakers, for giving me the freedom to go 'where the science took me', for being extremely generous with his knowledge, and for his advice to go for a run when writing got difficult. Learning about solar energy from Andrew has been an inspiring experience.

I would also like to acknowledge the support of the ANU Angus Nicholson Honours Scholarship for passion in science. I hope that this work can, in some way, honour the memory and passion of Dr. Nicholson.

Thankyou to all of the friendly solar community at ANU, in particular Dr. Evan Franklin who introduced me to the wonderful world of programming.

To the DE PhD students, thankyou (I think) for making me a better kicker player. Thanks also to my friendly Swiss officemate Lukas who helped me with Matlab.

To my past and present housemates, thanks heaps for putting up with me - particularly Wes; the copious amounts of red ink were greatly appreciated. Thankyou too to Rani, the best housemate I could ever have.

I am extremely thankful for the support of my family and friends. Mum and Dad, thankyou for everything. Thanks especially for letting me grow in the directions I have. To my unbelievably generous sister and new brother-in-law, who looked out for me the whole way through and supplied me with love packages when things were hectic, I can't thank you enough. I just hope I can repay you some day.

Finally, I'd like to give an enormous thank you to Gabriella for making this crazy year absolutely hilarious. I am so stoked we got to go through this together. Clockwork Gab, clockwork.

Abstract

Thermophotovoltaic systems are direct conversion heat engines that use photovoltaic cells to convert radiant energy from a heated object to electrical energy. Sources of heat for thermophotovoltaic (TPV) systems include sunlight, the combustion of fossil fuels, radioactive decay and industrial waste heat. Previous modelling indicated that thin photovoltaic cells were optimal for use in TPV systems. This thesis presents an original theoretical investigation into the application of thin silicon sliver cells in TPV systems.

Sliver cells are a novel type of photovoltaic cell fabricated from single crystal semiconductor wafers. They are bifacial, narrow and very thin - of the order of ten times thinner than current conventional cells. In addition, sliver cells have their metal contacts at the edges of the cell.

A computational model was constructed to examine and compare the performance of sliver cells with state-of-the-art conventional back-contact cells. Silicon was modelled as the semiconductor material due to the availability of modelling data and to provide an indication of the feasibility of thin silicon cells in TPV models. The model was validated using the semiconductor device modelling program PC1D under non-TPV conditions. Excellent agreement was observed. The analysis of silicon TPV cells was extrapolated to gallium antimonide.

It was found that sliver cells do not offer a clear advantage over well designed conventional cells in TPV systems. This was observed to be a result of horizontal carrier transport resistances across sliver cell widths. Minimum sliver widths in this study were limited to $300\,\mu$m. Within the assumptions of the model, sliver cell maximum TPV efficiencies $(32 \pm 2)\,\%$ were found to be $\sim 85\,\%$ of the maximum TPV efficiency achieved by conventional cells $(38 \pm 2)\,\%$. Sliver cell maximum output power densities $(600 \pm 30)\,\mathrm{mW/cm^2}$ were lower than those for conventional cells $(3300 \pm 100)\,\mathrm{mW/cm^2}$ by a factor of five.

Optimal cells for thermophotovoltaic systems were found to be thin back-contact cells with spectral filtering that reflected high-energy photons back to the emitter. The primary advantage for thin cells in TPV systems was observed to be a result of decreased resistive losses and not spectral considerations. It is from the original investigation of this thesis into the different resistance geometry of sliver cells in TPV systems that these effects can clearly be separated.

Practical considerations such as heat-sinking and cell-module circuitry were found to favour sliver cell geometries. Silicon cells were found to perform well at emitter temperatures that are above the current range of feasibility for TPV systems. Recommendations are made for the design of future TPV systems, potential fabrication processes for the manufacturing of optimal thermophotovoltaic cells are outlined, and the properties of future whole-system thermophotovoltaic models are discussed.

Contents

Chapter 1

Introduction

1.1 Overview

Over the past half-century, an elevated awareness of environmental sustainability has raised questions of our methods of electricity generation. Alternatives to fossil fuels have been increasingly considered as part of a solution to the issues of rising greenhouse gas emissions and resource sustainability. One such alternative is the conversion of solar energy to electricity through the use of photovoltaic cells.

Photovoltaic cells convert sunlight to electrical power. At present, they are not a cost-effective way of providing large scale electricity. In part this is due to sociological reasons; mostly it is due to the current costs of solar cell materials and the final output efficiencies of photovoltaic cells. In light of this, there is a broad research drive to reduce material costs and to increase photovoltaic efficiency.

There are theoretical limits to the efficiency with which solar cells can convert sunlight to electrical power. For conventional cells using direct sunlight the limit is 31 % – the Shockley-Queisser limit of detailed balance [1]. For fully concentrated sunlight the limit is 41 % [1, 2, 3]. There are ways to go beyond these limits. Two such methods include solar thermophotovoltaics (STPV) and multijunction stacks.

Solar thermophotovoltaics involves concentrating sunlight onto an intermediate absorber/emitter which radiates light with a colour-shifted spectrum to surrounding solar cells. Photons not absorbed by the cells are returned to the absorber/emitter, recycling energy. Multijunction stacks use stacked layers of cells, each with different energy bandgaps, assembled to collect more of the available spectrum.

The theoretical limits for STPV and multijunction conversion efficiency are very high at 85.4 % and 86.8 % respectively [2][3].

Multijunction cells with concentrated sunlight currently hold the record for solar energy conversion at 40.7 % [4]; they are considered a key part of the future of large scale solar energy generation. For solar thermophotovoltaics, the highest efficiency achieved is less than 15 % [5, 6, 7].

While research is still being undertaken for STPV [5-9] , a great deal of interest has been shown in thermophotovoltaic systems with non-solar sources of heat

A thermophotovoltaic converter is a direct-conversion heat engine that uses a photovoltaic cell to generate electric energy from thermal photons emitted by an adjacent radiating surface.

Sources of heat are not limited to solar radiation. Other sources include natural gas combustion, radioactive decay, vehicle engine heat, and industrial waste heat. Thermophotovoltaic (TPV) systems are currently being developed for use in homes for the co-generation of heat and electricity [10], and for use in deep space missions with radioisotope heat generation [11]. TPV systems are also of interest to the military, offering silent,

lightweight and portable means of electricity generation [9, 12, 13].

In thermophotovoltaic systems an object, typically a grey body or selective emitter, is heated to temperatures in excess of 1000 K. The resulting radiation is collected by surrounding photovoltaic cells. Photons not absorbed by the cells are reflected back to the emitter by a mirror behind the cells, thus conserving the emitter energy. Thermophotovoltaic geometries are significantly different to those of conventional flat-panel photovoltaic modules (figure (1.1)).

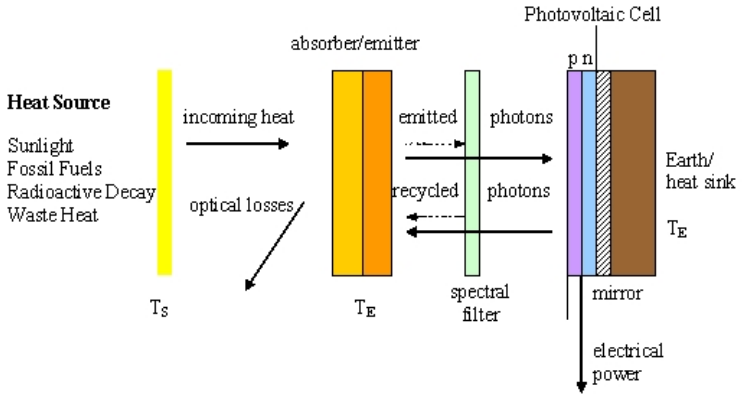

Figure 1.1: Schematic diagram of a thermophotovoltaic system. Photons not absorbed by the cell are able to be returned to the emitter.

Two key properties contribute to the potential high efficiency of TPV systems; 1) the emitter radiates less in the short-wavelength region of the spectrum where photovoltaic cells are inefficient and 2) long-wavelength photons that would not be effective in a conventional solar cell are recycled back to the emitter. This is illustrated in figure (1.2).

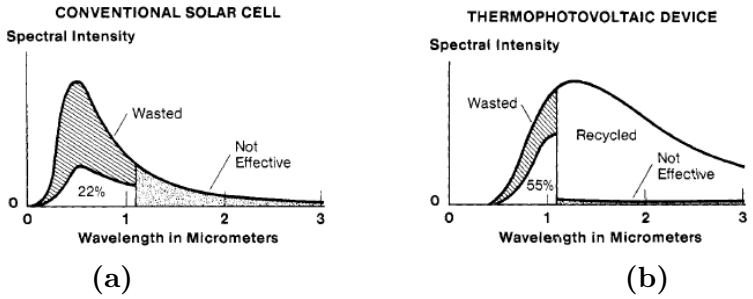

Figure 1.2: (a) Solar cell efficiency with sunlight spectrum. (b)Thermophotovoltaic cell efficiency with an incandescent spectrum. The vertical line within the spectrum represents the bandgap of the semiconductor material. Photons of shorter wavelength are absorbed by each cell, contributing to electrical output. Photons of longer wavelength are unable to be absorbed by the cell at all. In a conventional solar cell, these photons are ineffective, In a thermophotovoltaic device, the majority of these photons are reflected back to the emitter. A small proportion of long-wavelength photons are absorbed parasitically, this is represented by the dotted region in figure (b). Diagram from [14].

Current fuel-combustion TPV systems return chemical to electric efficiencies well below the $\sim 30\,\%$ efficiencies of typical diesel generators. The limitation of current TPV systems is primarily the photovoltaic conversion efficiency.

A strong research drive to find optimal TPV cell characteristics and increase TPV system efficiency is being undertaken. Previous modelling indicated that cells with thickness less than $100\,\mu$m would be optimal in TPV systems [14]. For conventional photovoltaic cells, $100\,\mu$m represents a lower practical limit of fabrication, even for high value applications such as TPV.

In 2000 a new method of fabricating photovoltaic cells was invented by Weber and Blakers at the Australian National University [15]. These cells, known as 'sliver' cells, are bifacial, narrow and very thin; ten times thinner than conventional technology (figure (1.3)). In addition, sliver cells have their contacts at the edges of the cell.

Figure 1.3: Sliver cells in this figure have a width of 1 mm, length 10 cm, and are $50\,\mu$m thick [16].

Sliver cells have potential applications in many different photovoltaic systems. This thesis examines the application of silicon sliver cells in thermophotovoltaic systems.

The two main properties of sliver cells that provide motivation for their application in TPV systems are their relative thinness and narrow width.

Being thin allows a reduction of 'free-carrier' absorption; the absorption of photons with energy $\epsilon < \epsilon_{bg}$, where ϵ_{bg} is the bandgap of the semiconductor material. This allows greater recycling of low energy photons. Having narrow width allows for intercell circuitry that reduces losses due to circuit resistance and non-uniform light distribution.

For this thesis, a computational model was developed to investigate the effect of cell thickness and geometry in realistic TPV systems. TPV system were considered for non-specific sources of heat. Modelling was undertaken with silicon as the semiconductor material due to the availability of accurate modelling data. While silicon is not an ideal semiconductor for TPV cells due to its relatively high bandgap of 1.12 eV, the material parameters for silicon photovoltaic cells are well established. Accurate device modelling with these parameters enabled a detailed examination of cell performance. In addition, silicon is far cheaper than alternative semiconductor materials and the investigation provided an indication of the feasibility of thin silicon cells in TPV systems. Modelling results for silicon are extrapolated to gallium antimonide TPV cells with energy bandgap 0.72 eV; the material currently being considered for TPV cells by most researchers due to its superior absorption response for lower blackbody temperatures.

Validation of the constructed computational model was undertaken with PC1D, a solar cell device modelling program developed at Sandia National Laboratories [17] suited to the detailed examination of semiconductor device processes. PC1D was not used directly because of the inherent two-dimensional nature of carrier transport in sliver cells. The agreement between the two models was found to be excellent. It is considered a central

element of this project that a model was developed that simulates photovoltaic cell devices with sufficient precision to engage in an analysis of thermophotovoltaic systems.

The performance of sliver cells was investigated and compared with the performance of state-of-the-art conventional cells. Before this project, sliver cells had not been investigated in TPV systems. The goal of this project was to fill that gap. In addition, the effects of blackbody temperature, spectral filtering, flat-band optical losses and cell temperature were investigated for TPV systems.

Within the range of parameters examined, it was found that sliver cells do not offer an advantage over well designed conventional cells in TPV systems. Sliver cell output power densities were observed to be strongly limited by carrier transport resistance across the sliver cell width. Optimal cells for thermophotovoltaic systems were found to be thin back-contact cells with spectral filtering that reflected high energy photons back to the emitter. Silicon cells were found to perform well at emitter temperatures that are above the current range of feasibility for TPV systems.

Important parameters that are identified for the future development of TPV systems include cell contact geometry, material resistivity, flat optical losses and cell temperature.

1.2 Thesis plan

In Chapter 2 we introduce photovoltaic cell operation. This includes an introduction to semiconductor materials, the formation of the p-n junction and the components of the solar cell equation. Following this is a comparison of the characteristics of conventional cells and sliver cells. A background introduction to thermophotovoltaic systems is presented in the second part of this chapter. This includes a review of current TPV system designs and an analysis of TPV material properties and system efficiencies. The current limitations to TPV performance are discussed and the motivations for this project are presented.

In Chapter 3 we review the alternative methods of solar cell modelling. The three broad approaches to TPV modelling are outlined, and their suited applications are discussed. The requirements for TPV modelling in this project are presented and the selected model is outlined. The applicability and limitations of the selected model are discussed.

Chapter 4 presents the methods of the TPV system simulation. The calculations of the device processes are outlined in detail, and the structure of the TPV system, antireflection coating, and back surface mirror are reviewed and presented. The technical material parameters chosen for each cell thickness are optimised and discussed, and the extrapolation techniques for the material data are reviewed. The chapter concludes with a discussion of uncertainty.

The results of the modelling are presented in Chapter 5. Firstly, the chapter presents the validation of the model. Following this is an examination of an ideal TPV system at constant incident power density. The effects of spectral filtering, flat optical losses and cell temperature are examined in this system alongside the analysis of optimum cell thickness and emitter temperature. An original analysis of the application of Sliver Cells to thermophotovoltaic systems is presented with a comparison to current state-of-the-art conventional cells. The cells are modelled in a TPV system in which incident power density is optimised for each cell thickness and emitter temperature. The modelling results are then summarised, and an extrapolation to gallium antimonide TPV cells is considered. TPV issues outside those modelled are investigated and the optimal cell for use in TPV systems is discussed.

We conclude with a summary of the work presented in this thesis, and a discussion of possible future research directions in the three areas of TPV system design, optimal TPV cell fabrication, and whole-system thermophotovoltaic modelling.

Chapter 2

Photovoltaic Cells and Thermophotovoltaic Systems

This chapter introduces photovoltaic cells and thermophotovoltaic systems. First, a brief description of semiconductor materials is presented and the formation of the p-n junction is outlined. This is followed by an introduction to photovoltaic cell operation, the solar cell equation and the processes determining internal quantum efficiency and transport resistance. Conventional photovoltaic cells and sliver cells are then described and compared, and the motivations for the analysis of sliver cells in thermophotovoltaic systems are discussed. The second part of the chapter introduces the concept of thermophotovoltaic systems. A review of TPV development is presented, followed by an analysis of current TPV systems and a discussion of their limitations.

2.1 Photovoltaics

Photovoltaic cells generate electricity through the absorption of light. Conventional photovoltaic cells consist of a p-n junction diode made from semiconductor materials. Semiconductors are materials that have small but non negligible densities of free charge-carriers at thermal equilibrium. These carriers are of both negative charge (electrons) and positive charge (holes). In semiconductor physics, a hole is an absence of an electron in the valence band of the semiconductor, they can be considered as free, positively charged particles that effectively move by the corresponding motion of an adjacent valence band electron. Both holes and electrons contribute to current flow in a semiconductor.

2.1.1 The p-n junction

In undoped semiconductors at constant temperature with no external excitation (thermal equilibrium), the number of free electrons and holes are equal. This ratio can be altered by the introduction of impurities into the semiconductor. Doping the semiconductor so that there are higher numbers of free electrons results in an n-type material. Silicon is a commonly used semiconductor with four outer electrons. Doping silicon with phosophorus, having five electrons in its outer shell, results in n-type silicon. Similarly, doping silicon with boron, having three outer electrons, leads to higher numbers of free holes in the semiconductor, resulting in p-type silicon.

The level of doping affects the resistivity of the semiconductor material, the carrier mobilities, and the lifetimes of the minority charge carriers. These are key parameters of PV cell materials.

Creating n-type and p-type materials directly adjacent to each other results in strong carrier diffusion gradients and a significant electric field across the narrow region between

the two materials, known as the p-n junction. The electric field across this region is the basis of the diode, and can be used to extract useful current from a photovoltaic cell.

2.1.2 Photon absorption

Semiconductors absorb photons with energy $\epsilon > \epsilon_{bg}$ where ϵ_{bg} is the bandgap of the particular material. The bandgap energy is the energy difference between the conduction and valence bands of the semiconductor. This bandgap energy is particular to each material; for silicon $\epsilon_{bg} = 1.12\,\text{eV}$, for gallium arsenide it is 1.42 eV and for gallium antimonide 0.72 eV [18]. The corresponding bandgap wavelengths are 1100, 870 and 1700 nm, respectively. Absorption processes in a semiconductor are outlined in figure (2.1).

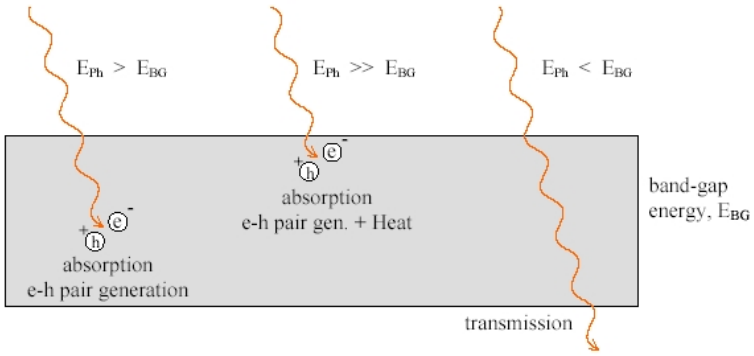

Figure 2.1: The absorption processes of a semiconductor material. For high energy photons $\epsilon \gg \epsilon_{bg}$, the excess energy above the bandgap is lost in thermalisation. For photons with energy lower than the bandgap, the semiconductor is mostly transparent. A small number of photons $\epsilon < \epsilon_{bg}$ are absorbed by free-carriers; a process known as free-carrier absorption. The absorption coefficients for each photon wavelength are characteristic to each semiconductor material [16].

2.1.3 Photovoltaic cell operation

When a photon is absorbed by a photovoltaic cell, an electron-hole pair is generated. In a good cell, these charges are separated by the electric field across the p-n junction and collected by the cell's negative and positive contacts respectively. Some electron-hole pairs recombine within the semiconductor material before reaching the contacts. The performance of a cell is strongly dependent on the rate of recombination of minority charge carriers within the semiconductor material, where 'minority' charge refers to electrons in p-type material, and holes in n-type material. The recombination rate is characterised by the average duration or distance that a minority carrier survives for before recombining; the minority carrier lifetime or diffusion length respectively.

The rate of recombination is dependent on the number of impurities and defects within the cell and cell surface. Higher doping leads to lower minority carrier lifetime and less collection of carriers for use in the external circuit, but may also allow for higher open-circuit voltage and fill factors (outlined below). The efficiency with which photon absorption leads to the useful collection of charge carriers is known as the internal quantum efficiency (IQE).

Conduction of charge carriers through the cell results in ohmic resistance losses. Cell resistivity is inversely dependent upon doping, leading to a trade-off between higher IQE, lower open-circuit voltages and increased transport resistance. This balance is observed to be important in Chapters 4 and 5.

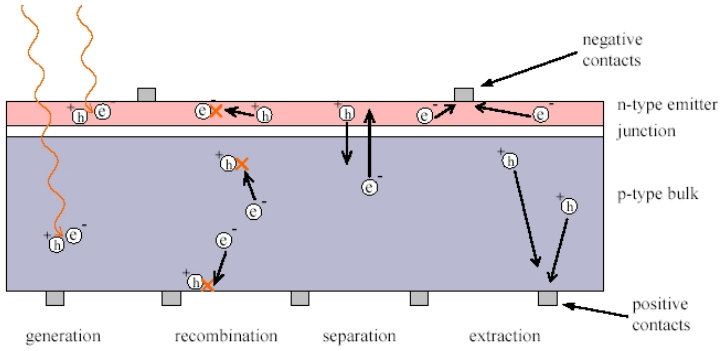

Figure 2.2: Diagram of the four main processes of a photovoltaic cell with p-type bulk and n-type emitter. The processes of recombination and transport resistance adversely effect cell performance [16].

2.1.4 The solar cell equation

When light is incident on a photovoltaic cell with its electrical contacts shorted by a connecting wire, a current is present. This current per cross-sectional unit area is known as the short-circuit current density J_{sc} with conventional units of A/cm^2. The equation governing normal photovoltaic cell operation is the sum of the photo-induced current density and recombination current density components. The recombination or diffusion component is dependent on the voltage across the cell, the temperature of the cell and a quantity known as J_0, the reverse saturation current density. J_0 is dependent on the doping, minority carrier lifetime and surface characteristics of the cell.

$$J = J_0(e^{\frac{qV}{kT}} - 1) - J_{sc} \tag{2.1}$$

The left hand term is the ordinary diode equation governing the diffusion of carriers across a p-n junction under forward bias. The right hand term is the current caused by illumination and is oppositely directed to the diffusion current. The voltage at which no current flows across the cell is known as the open circuit voltage V_{oc}. The relationship between voltage and current in a photovoltaic cell can be seen in figure (2.3).

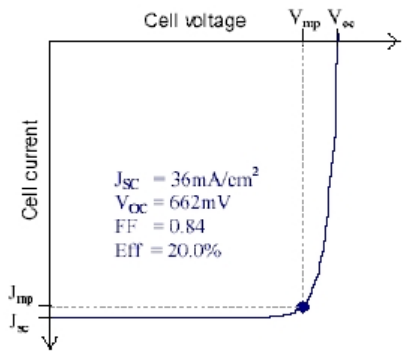

Figure 2.3: Current voltage (I-V) characteristics of a very good solar cell under normal sunny conditions (0.1 W/cm^2). The fill factor (FF) relates V_{oc} and J_{sc} to the maximum power point(mp) of the cell. Cell diagrams courtesy of Evan Franklin [16]

The maximum power output of the cell is then $V_{mp} \cdot J_{mp}$, which are related to V_{oc} and

J_{sc} through the fill factor; a measure of the 'squareness' of the I-V curve shown in figure (2.3). The fill factor is dependent on the internal resistances of the cell and is calculated:

$$FF = \frac{V_{mp} \cdot J_{mp}}{V_{oc} \cdot J_{sc}} \tag{2.2}$$

The final efficiency of the cell is then given:

$$\begin{aligned} \eta_{cell} &= \frac{P_{out}}{P_{in}} \\ &= \frac{V_{mp} \cdot J_{mp}}{P_{in}} \\ &= \frac{FF \cdot V_{oc} \cdot J_{sc}}{P_{in}} \end{aligned} \tag{2.3}$$

For a more detailed description of photovoltaic cell operation, the interested reader is referred to the excellent introductions in the texts of Kittel [19] and Sze [20].

2.2 Conventional photovoltaic cells

The geometry of conventional photovoltaic cells is similar to that presented in figure (2.2). A typical conventional cell has thick, lightly doped bulk with positive contacts at the rear, and a heavily doped emitter with negative contacts at the surface. Many advances have been made with this technology [21, 22, 23], and the current single junction Si efficiency record of 24.7 % is with cells of this structure [24].

Additional cell structures have been manufactured that yield very high efficiencies through reduced parasitic reflection from the top metal contacts. These cell structures are buried-contact and back-contact cells, as illustrated in figure (2.4).

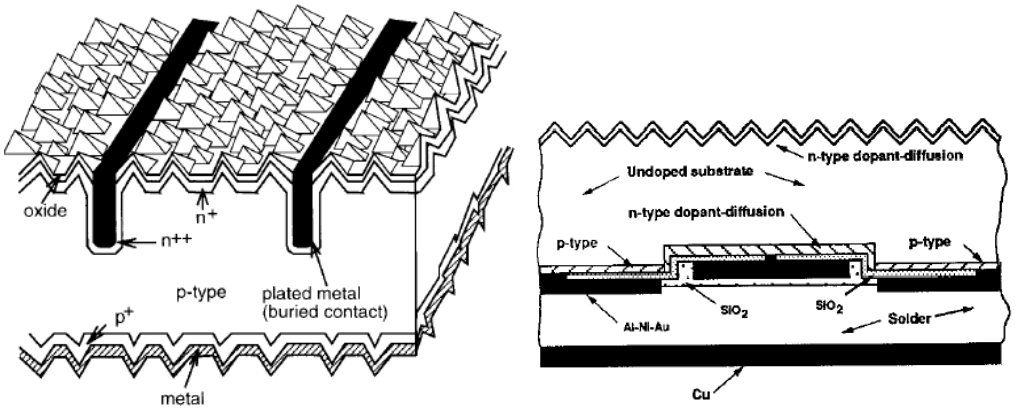

(a) **(b)**

Figure 2.4: (a) Three dimensional picture of a buried contact cell developed at the University of New South Wales [25]. (b) Cross section of a back-contact cell developed at Stanford University [26].

An ideal cell with back-contact structure and almost no parasitic reflection was chosen as the structure representing conventional cells for our analysis of TPV systems.

An early theoretical study by R. Swanson in 1978 indicated that the optimal thickness for silicon cells in thermophotovoltaic systems was $\sim$ 25 μm [14]. The thickness of conventional photovoltaic cells is currently $\sim 200\,\mu$m, with the possibility of 100 μm thicknesses for high value applications. The limit of thickness is due to the process of cutting semiconductor wafers from a single ingot.

Cell materials form a large proportion of solar cell cost. As a result, an intense research drive is being undertaken in what is known as second-generation photovoltaics; thin-film technology that provides advantages in both TPV and PV solar energy. Second generation technology includes dye-sensitized solar cells, crystalline silicon on glass, and epitaxial growth of cells on matched semiconductor substrates. A large amount of research is also being undertaken in third-generation photovoltaics; cells that move beyond the standard diode configuration of solar cells. Martin Green's book *Third Generation Photovoltaics* (2003) presents a detailed introduction to these. While significant advances are expected in the future, second and third generation technologies still return much lower efficiencies and power densities than first generation photovoltaic cells.

2.3 Sliver cells

In 2000 a new method of fabricating photovoltaic cells was invented by Blakers and Weber at the Australian National University [15]. These cells, known as Sliver cells, are processed within the wafer and are later micromachined out to form many individual slivers. Sliver cells are thin, flexible, bifacial and have their metal contacts on the edges of the cell as illustrated in figure (2.5).

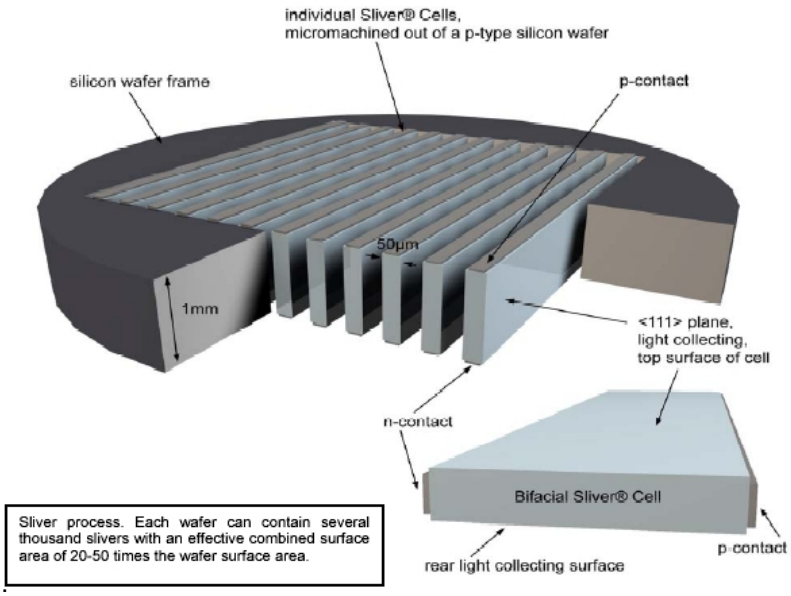

Figure 2.5: Diagram of Sliver Cell Fabrication [15].

There are three main properties of sliver cells that are substantially different to conventional solar cells. Firstly, sliver sells are able to be made very thin; 10 - 50 μm. Secondly, sliver contacts are at the edges of the cell, and thirdly, slivers are bifacial; allowing incident light on both surfaces (figure (2.6)).

Being thin (of the order of ten times thinner than conventional cells) allows for a reduction in parasitic free-carrier absorption. Free-carrier absorption is the absorption of photons with energy $\epsilon < \epsilon_{bg}$, by the free charge-carriers within the cell, and does not

contribute to the electrical output power of the cell. Free-carrier absorption is especially important in TPV systems where photons of $\epsilon < \epsilon_{bg}$ are reused. Being thin also results in a higher proportion of photons with energy $\epsilon \gg \epsilon_{bg}$ being absorbed by the cell. This results in a waste of photon energy (as illustrated in figure (1.2a)), and is referred to as blue-loss. Blue-loss for thin cells is due to the absorption structure of most semiconductor materials; high absorption coefficients (with units of photons/cm) for short wavelengths, decreasing for longer wavelengths towards the bandgap. The absorption coefficients for silicon and gallium antimonide are presented in Chapter 4.

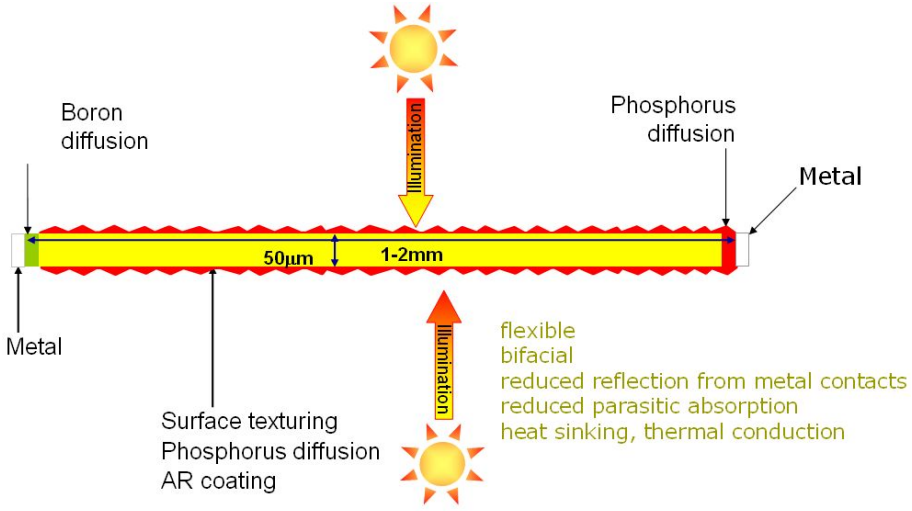

Figure 2.6: Cross-section of a Sliver Cell, with possible illumination from both sides [15].

Current sliver cells have typical length 5 - 12 cm, width of 0.5 - 2 mm, and thickness 20 - 100 μm. Possible sliver width may be reduced to $\sim 300\,\mu$m, and the thickness range increased to 10 - 1000 μm [27].

Having contacts on the edge of the cell reduces parasitic reflection from the cell surface and allows more light to be incident on active cell area. Metal contacts on the edges also allows for greater thermal contact to a heat sink; another important consideration for concentrated photovoltaic systems.

In addition, having contacts at the edge of the cell results in a different transport resistance geometry. Instead of charge carriers being transported vertically, as in a conventional cell, charge carriers are transported laterally through the cell. This is observed to be of key importance for systems operating with high illumination densities. Franklin (2006) observed this effect to be significant for sliver cells in concentrator systems [16], and it is observed to be an important consideration for sliver cells in TPV systems.

The two properties of thinness allowing reduced free-carrier absorption, and having contacts at the edge reducing surface relection and increasing thermal conduction, were the original motivations for the analysis of sliver cells in TPV systems.

2.4 Thermophotovoltaics

In 1956 Dr. Henry Kolm at MIT's Lincoln Laboratory used a Coleman camping lantern with an incandescent gas mantle and a silicon solar cell to create what is considered the first thermophotovoltaic system [28]. The system had an output power of approximately 1 Watt, with a total system efficiency of less than 1 %. The field has progressed significantly since then.

At MIT in 1960-61 Prof. Pierre Aigrain gave a series of lectures on the potentials of TPV design, after which followed a substantial research effort in the field. TPV systems offer high power density, silent operation, fuel versatility and low maintenance requirements. They have potential applications in remote power generation, cogeneration with heat in domestic gas furnaces, large scale recovery of high temperature industrial waste heat, and military and space power generation. It was the military and space applications that initially drove research in the field; and they continue to do so today.

Through the 1960s, US Army research pursued a system that could deliver 500 W in a lightweight portable unit. Although proof of concept systems were built, the military's requirements were not met and in the mid 1970s military interest in TPV slowed considerably [12, 29].

It is only in the last decade that TPV systems have regained favour. This is mainly due to the increase in PV efficiency, advances in concentrator systems, and the development of low bandgap semiconductor materials such as gallium antimonide and germanium.

The TPV systems that are being developed today (figures (2.7a) and (2.7b)) comprise of cells made of these materials and selective emitters spectrally matched to the cell bandgaps.

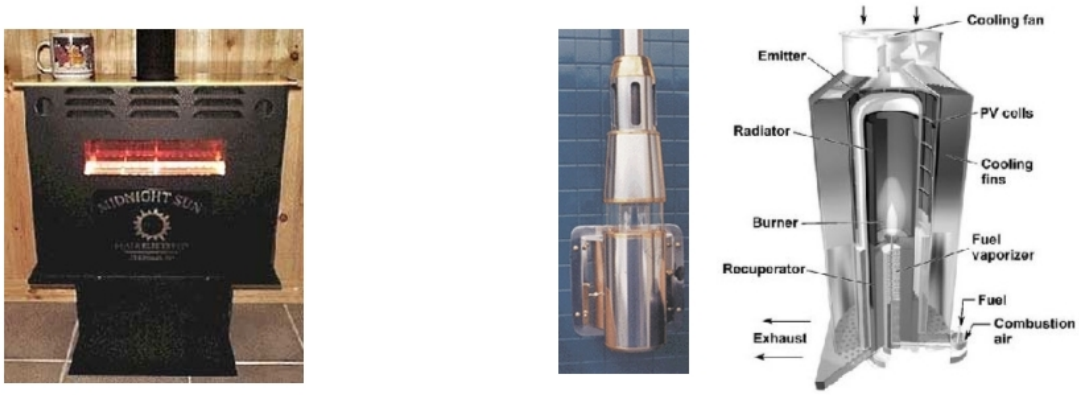

(a) **(b)**

Figure 2.7: **(a)** The Midnight Sun system developed by JX Crystals for the generation of heat and electricity in residential homes. **(b)** left) a prototype system designed for use in recreation vehicles [10], right) the internal design of a cylindrical TPV system from McDermott Technology [30].

The fuel-to-electric efficiencies of current systems is quite low. The maximum predicted efficiency for current Midnight Sun systems is 12 %, and for radioisotope TPV it is 16 % [13, 30]. In comparison, medium sized diesel generators operate at fuel-to-electric efficiencies greater than 30 %.

Similarly for solar-thermophotovoltaic systems; the two systems that have been built beyond proof of concept designs operate at *thermal-to-electric* efficiencies of less than 30 %; this is the efficiency with which the system converts electrical power from the thermally radiated power of the emitter. Solar-to-electric efficiencies are less than 10 % [6, 8].

There are mixed opinions about the future of STPV. From a consideration of greater return efficiencies of sub-bandgap photons, higher concentrations of light, and more selective emitters, *Andreev et al* estimate that "these approaches together should increase the STPV system efficiency up to 30 % and higher" [5].

Timothy Coutts, editor of the first five proceedings of the NREL TPV conferences,

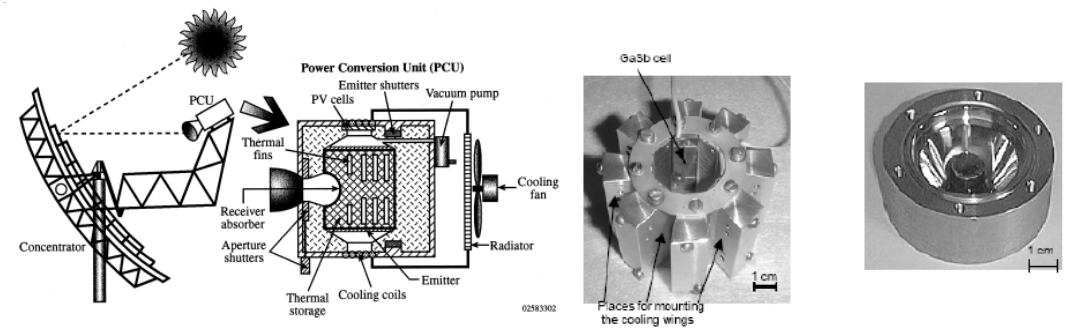

(a) **(b)**

Figure 2.8: (a) Schematic of the STPV system designed by Stone *et al*[6], (b) The TPV conversion units designed by Andreev *et al* [**?**]

questions the approach: "With solar-powered TPV, one may ask, 'why is the sunlight itself not used?', reasoning "...if a similar concentration ratio were used [directly] on high-efficiency solar cells, the power density output would be much greater"[9].

This reflects the wider view; even with an extremely high thermal-to-electric efficiency of 50 %, the losses associated with solar concentration and emitter heating would be sufficient to reduce STPV efficiencies to below those already obtained by multijunction concentrator cells.

Nonetheless, due to the ability of STPV to store solar energy in thermal mass and its potential use in co-generation systems, interest in STPV systems is still vibrant: McDonnell Douglas Aerospace are committed to the technology and believe "that STPV is a viable power system for both space and terrestrial power applications"[7], and research in Europe is still actively pursuing the technology [5, 31].

For TPV systems of any heat source, advances in the efficiency of conversion of heat energy to electrical power are intensively being sought.

2.4.1 Current TPV limitations

The theoretical efficiency limit of a TPV system is the Carnot efficiency: $\eta = 1 - T_{cell}/T_{emitter}$. This is reached through the consideration of an ideal cell with only radiative recombination, in an ideal TPV system with a monochromatic filter at the bandgap energy of the cell [2, 3, 23].

Current TPV systems have efficiencies very much less than the Carnot limit. The main limiting factors of TPV systems are identified as spectral filtering, cell conversion efficiency, and adequate systems modelling [13, 30, 32, 33].

Spectral filtering involves adjusting the spectrum incident on the cell to maximise the absorption of photons just above the bandgap energy. As outlined previously, the absorption of photons with energy less than the bandgap does not contribute to output power, and the excess energy of photons with much higher than the bandgap is lost to thermalisation (figure (1.2)).

Spectral filtering can occur in four stages; each, when optimised, has the effect of recycling unwanted photons back to the emitter. The first stage is to use a selective emitter, such as silicon carbide or various rare-earth oxides, that radiates with a spectrum matched to the absorption structure of the cell. Secondly an intermediate filter may be used, allowing optimal photons through to the cell and reflecting all others back to

the emitter. Thirdly an antireflective coating can be applied directly to the cell surface. Fourthly, and of interest to this project, spectral filtering can occur with cell thickness; reducing cell thickness allows for a reduction in free-carrier absorption of photons with energy $\epsilon < \epsilon_{bg}$. This thesis investigates the use of cell thickness in spectral filtering and the relative importance of above and below bandgap filtering.

To increase cell conversion efficiency, intrinsic cell characteristics such as material doping levels and region thicknesses need to optimised. This has not yet been done for TPV cells. Partly this is due to the wide range of conditions in which TPV systems operate. It is also due to the relatively recent development of low-bandgap III-V semiconductor compounds suitable for TPV systems. This thesis examines the optimal cell characteristics for silicon, and interprets these parameters for gallium antimonide.

In TPV systems there are a broad range of inter-related parameters that affect final TPV efficiency. For example, incident illumination and levels of spectral filtering alter optimal material cell characteristics, and vice versa.

To investigate the parameter ranges for which TPV systems are most efficient, accurate modelling of TPV systems is required.

Chapter 3

Thermophotovoltaic Modelling

This chapter reviews the various methods of TPV systems modelling. The three broad categories of TPV modelling: ideal theoretical modelling, detailed device modelling, and whole systems modelling, are outlined and their relevant applications are discussed. The properties of the model required for this project are discussed and the techniques of Monte Carlo simulations and linear systems programming are reviewed. The chapter concludes with an outline of the model utilised for this project and a discussion of its application.

3.1 Analytical TPV modelling

Early work by de Vos [2], Harder and Wurfel [3] and Swanson [14] demonstrated the potential efficiencies of TPV systems. Initial work concentrated on solar thermophotovoltaics, and was driven by the very high theoretical efficiency limit of 85.4 %.

This efficiency limit considers a STPV system as a Müser engine converting sunlight incident on earth into work [2].

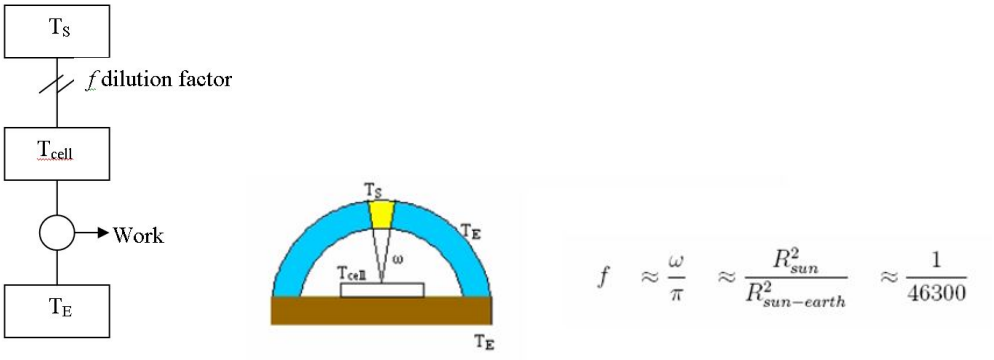

Figure 3.1: (a) Schematic representation of a Müser engine, (b) View factor of a solar cell on Earth, f is the aperture at which the cell views the Sun. Concentration increases the value of f.

Here, the cell is an absorber/emitter with a bandgap, such that it completely absorbs photons with energies $\epsilon > \epsilon_{bg}$ and reflects for $\epsilon < \epsilon_{bg}$. With C as the concentration of sunlight, the heat flow to the cell is then given by [2]:

$$Q_1 = \frac{2\pi}{c^2h^3}\left(Cf\int_{\epsilon_g}^{\infty}\frac{\epsilon^3 d\epsilon}{exp(\frac{\epsilon}{kT_S})-1} - (1-Cf)\int_{\epsilon_g}^{\infty}\frac{\epsilon^3 d\epsilon}{exp(\frac{\epsilon}{kT_E})-1} - \int_{\epsilon_g}^{\infty}\frac{\epsilon^3 d\epsilon}{exp(\frac{\epsilon}{kT_{cell}})-1}\right) \quad (3.1)$$

The STPV theoretical efficiency maximum is reached by considering the cell as a Carnot engine, limited only by radiative recombination. For unconcentrated sunlight, the efficiency maximum is 53.6 % at T_{cell}=865 K with an optimal bandgap of 0.9 eV [2] [3]. For full concentration the efficiency maximum is 85.4 % at T_{cell}=2544 K [2] [3]. In the literature this concentration factor is presented without much disclaimer. It is important to note, however, that full concentration can only be achieved with a segment of an enormous ellipsoidal mirror set in space, shaped to have the Sun and Earth at each focus [2].

Concentration does still increase system efficiency, giving a maximum of 85.4 %; the theoretical limit of efficiency for a single engine converting solar radiation to work at the Earth's surface.

Analytical modelling of non-solar TPV systems proceeds in a similar manner; through the consideration of cell devices as Carnot engines limited only by radiative recombination. Cody *et al* (1999) analyze such a system, and for blackbody emitter temperatures arrive at maximum efficiencies between 30-35 % and optimum bandgaps between 0.2-0.5 eV. Similar studies were done by Burger and Mueller (1994) [34] and El-Husseini and Gray [35] (1994). Analytical modelling is a highly idealised approach, well suited for finding optimal semiconductor materials and emitter temperatures for TPV systems. It is also useful in providing a limit towards which systems, in principle, can improve. The approach is not as suited for the analysis of optimal realistic cell characteristics and whole system design.

3.2 Device modelling

Detailed device modelling has been developed over many years for the optimisation of solar cell performance. The approach consists of numerically solving the full set of coupled non-linear semiconductor equations with a defined set of boundary conditions. These equations are the Poisson charge neutrality equation, the electron and hole continuity equations, and the electron and hole transport equations. The full set are presented in Appendix A.

There are numerous models that have been developed for this method of semiconductor device analysis. Two examples are PC1D, a program developed by P. Basore at Sandia National Laboratories that solves the semiconductor equations in one dimension [17], and DESSIS, a piece of semiconductor modelling software from Integrated Systems Engineering (ISE) capable of modelling semiconductor devices in two or three dimensions.

Figure (3.2) represents the characteristics for which this type of modelling is suited; detailed examination of carrier transport and analysis of the specific regions of cell efficiency losses. In addition, models that numerically solve the semiconductor equations are able to provide a detailed picture of material performance, carrier recombination and cell resistance.

These models have been engaged to analyze silicon (Si) gallium antimonide (GaSb) cells in TPV systems. GaSb is being modelled since it has a bandgap of 0.72 eV which is well suited to realistic TPV system temperatures of 1200 - 2400 K. In addition, GaSb is

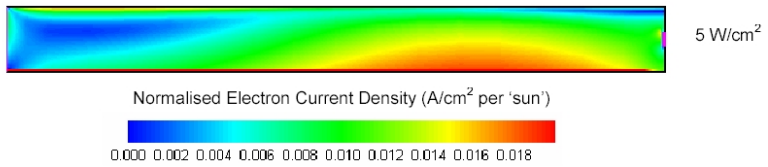

Figure 3.2: An example of DESSIS modelling of photovoltaic cells. The above is a 2D cross-section of electron current density in sliver cells under $5\,\mathrm{W/cm^2}$ illumination intensity, modelled by Franklin (2006) [16]. The cross section is vertically through the sliver cell, with sliver width and thickness as the x and y axes respectively.

able to be manufactured without using epitaxial techniques and is easily doped with zinc and tellurium to form p-type and n-type structures respectively . It is considered one of the most suitable materials for use in TPV systems [29].

Semiconductor models are being used to find the GaSb optimal material characteristics such as doping levels, emitter diffusion depths, and surface and contact oxides [36-41] .

Supplementing this work has been research on the detailed material parameters that semiconductor device modelling relies on. These include temperature coefficients for carrier mobilities, intrinsic carrier concentrations, and recombination lifetime limits [33, 42].

The semiconductor equation approach of modelling is well suited for the detailed examination of cell performance; indeed PC1D was used extensively in this project to obtain optimal material parameters and to validate the modelling of cell output characteristics.

However, detailed device modelling it is not well suited for application to whole TPV systems. This is due to the difficult and cumbersome nature of incorporating different stages of spectral filtering, multiple photon reflections and reabsorption by the emitter.

It is a slight 'catch-22' in that system configuration can not be optimised without knowledge of cell performance, and that cell performance can not be optimised without knowledge of system configuration. Cell performance is sensitively dependent on illumination intensities and incident spectra.

Until recently, the lack of knowledge about GaSb cell performance led to a concentration of effort on cell device characteristics; "Nearly all [TPV] work undertaken to date has concerned the optimization of individual components ... with relatively little being devoted to the system as a whole"(Coutts (2001), [32]).

Linear programming and Monte Carlo methods have since started to address this issue.

3.3 TPV system modelling

There are two approaches to whole systems TPV modelling. The first is to treat the photon paths linearly through the system, in one-dimension. This involves modelling each of the TPV processes outlined in figure (1.1) as angularly independent, and tracking the path of photons of different energies as they move through the system. Linear models simulate the energy transfers of the system beginning with emission from the radiating surface and ending with absorption in a medium - which could be the cell, or mirror, or the emitter itself.

The second approach is Monte Carlo modelling (MCM), which allows the extended tracing of photons in two and three dimensions. This is especially useful in the modelling of complete TPV systems with non uniform radiation by the emitter and angle dependent cell absorption and transmission coefficients. The effects of module geometry and cell surface texturing are also well suited to Monte Carlo modelling. Texturing involves altering of the cell surface to increase the absorption of light; the cell presented in figure (2.4) displays

a significant level of texturing. As with linear models, Monte Carlo modelling involves tracking the path of a number of photons beginning with radiation from the emitter, and ending in absorption by a medium.

From early work by Cashwell (1959) on "Monte Carlo for random walk problems" [43] and Moglestue (1993) "Monte Carlo simulation of semiconductor devices" [44], Monte Carlo methods have begun to be developed for TPV systems. One such model, developed by Aschaber *et al* (2003) [45] simulates an ideal TPV system using the RACER-X photon-tracing program, and to first approximation considers different TPV geometries and heat conduction from the PV module.

The ability to model these detailed processes comes at a computational price. Aschaber *et al* in the paper that presented their model, also present the complexity tradeoff for Monte Carlo methods in figure (3.3).

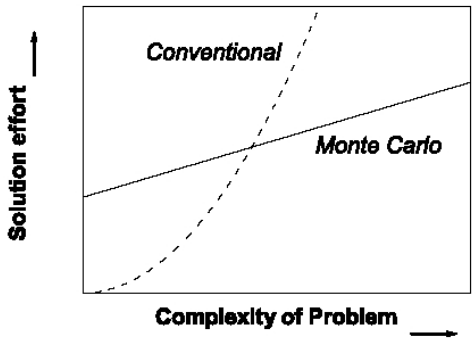

Figure 3.3: A comparison of Monte Carlo and conventional solution techniques presented in Aschaber *et al* (2003) [45].

3.4 Modelling sliver cells in TPV systems

There were three main requirements for modelling and comparing sliver cells with conventional cells in TPV systems. Firstly, the model needed to be able to simulate lateral resistive losses within photovoltaic cells. Secondly, the model needed to simulate different spectral filtering techniques, back-mirror reflectivities and flat wavelength-independent surface reflections in the TPV system. And thirdly, the model needed to be able to track the complete histories of photons from emission through to potential reabsorption from the radiating surface, including multiple reflections within components.

The modelling of cells with realistic recombination parameters, and achievable system components, limited the application of the analytical approach.

The first requirement limited the application of one-dimensional semiconductor models such as PC1D, since lateral resistance in sliver cells is inherently a 2-Dimensional process.

Furthermore, the cumbersome nature of applying multiple reflections and photon tracking in detailed semiconductor device models, makes the use of 2D and 3D modelling programs such as DESSIS, unsuitable.

The aim of this project was to analyze sliver cell performance in TPV systems and the use of cell thickness as a spectral filter for sub-bandgap photons, with sufficient precision to draw conclusions, but without attempting a precision beyond the scope of an honours project.

Monte Carlo modelling techniques are able to simulate cell performance and spectral filtering. In addition, MCM techniques allow the simulation of the effects of TPV emitter

geometry, module design and cell heat conduction, and the optimisation of each of these components in complete TPV systems.

However, with reference to the solution complexity curve of figure (3.3), for the simple and more focused analysis of sliver cells in TPV systems, a linear model was chosen for this project. A discussion of optimal modelling techniques for complete TPV systems is presented in section (6.2).

The constructed model, presented in the following chapter, is similar to a simplified Monte Carlo model in that the histories of a number of photons are tracked. The key difference is that the paths of the photons are restricted to one dimension, and that the angular dependence of absorption, reflection and transmission processes are neglected. The two-dimensional carrier resistive losses of sliver cells are still able to be modelled; since it is only the path of *photons* that are restricted to one dimension.

While Monte Carlo methods are excellently suited to complete TPV systems analysis and optimisation, for the reduced focus of modelling cell thickness and sliver cell performance in TPV systems, the constructed model was found to perform exceptionally well.

Chapter 4

Methods

This chapter discusses the methods of analysis for the project. It begins with an overview of the modelling approach and a discussion of the use of silicon. Following this is an outline of the paths of photons through the system and a presentation of the model schematic. Next, the more technical aspects of the model are discussed in detail. Device characteristics such as reverse saturation current density, short-circuit current density, open-circuit voltage and fill factor calculations are presented and the series resistance calculations for both sliver cells and conventional cells are outlined and discussed. Following this, the technical material parameter selections are presented. This includes bulk and emitter optimal resistivities, mirror reflectivity, and antireflection coating selection. The optimisation and extrapolation techniques are also outlined. The chapter concludes with a discussion of uncertainty.

4.1 Methods overview

As presented in the introduction, the central aim of this project was to investigate sliver cells in TPV systems and compare them to the performance of state-of-the-art conventional cells. To enable this, achievable TPV systems parameters needed to be modelled to allow realistic indication of cell performance. This principle guided model design and parameter selection throughout the study.

As a result it was decided that the effects of non-uniform illumination were to be modelled separately from cell performance; cell-external effects are discussed in section (5.9). In addition, the semiconductor material of the modelled cells was chosen to be silicon (Si) and not gallium antimonide (GaSb).

As outlined in section (1.1), silicon was chosen for two main reasons. The first is "the lack of a reliable and accurate set of GaSb material parameters as input for the semiconductor simulation tools." (Martin and Algora, 2004 "Key issues for an accurate modelling of GaSb TPV converters" [42]). While recent work has since started to address this, the set of optimal GaSb doping levels and corresponding carrier lifetimes and diffusion lengths are still not established. Doping levels, recombination rates and diffusion lengths are critical parameters for a project examining the effect of cell thickness. The range of material parameters for Si photovoltaic cells are thoroughly known, ensuring that a clear picture of cell performance is obtained, less masked by material parameter uncertainties. In addition, accurate modelling data allowed the use of PC1D for the validation of the model. This enabled a detailed check of the TPV model cell performance calculations.

Secondly, silicon is interesting in its own right. Its bandgap is too high to be optimal, however, silicon cells are far cheaper, through mass production, than alternative semiconductor materials. The investigation into Si cells in TPV systems provides an indication of whether the reduced efficiency of silicon may be compensated by low material

costs. Silicon also provides a test of the model, and a platform for the analysis of other semiconductor materials.

Gallium antimonide and other low-bandgap III-V semiconductors are currently the materials of choice for TPV systems. This is due to the better spectral response of these materials at longer wavelengths. GaSb, with bandgap energy 0.72 eV absorbs more of the blackbody spectrum at 1200-2400 K than Si, having a bandgap of 1.12 eV.

For this reason, Si cells are investigated at TPV emitter temperatures between 1200 and 4200 K. Current TPV systems operate at temperatures 1200 - 2400 K. While temperatures in excess of 3000 K are not currently feasible for TPV operation, the analysis of high blackbody temperatures allows an examination of optimum silicon cell performance, and a reference for the extrapolation to GaSb cells.

The extrapolation is found to be reasonable; the absorption coefficient structures of Si and GaSb are similar (figures (4.7) and (4.8)), and silicon responds to blackbody temperatures of 2200-3400 K in a similar way as gallium antimonide with temperatures of 1200-2400 K. In addition, the resistive structure differences between sliver and conventional cells have the same effect for Si cells as for GaSb. The interpretation and extrapolation of the results for gallium antimonide cells is presented in section (5.10).

4.2 Photons through the TPV system

The first step of the computation model is to generate a standard blackbody spectrum:

$$P_{BB}(\lambda, T) = \left(\frac{2\pi hc^2}{\lambda^5}\frac{1}{e^{\frac{hc}{\lambda kT}} - 1}\right)\left(\frac{1}{10000}\right)\Big(f(T, \eta)\Big) \tag{4.1}$$

The first term is the planck spectrum of power density per unit surface area per unit wavelength (with units in J/(s.m^2.m)). The second term converts the spectrum to the conventional units in solar cell physics of W/(cm^2.m). The final term is a dilution factor, where $f(T, \eta)$ is the ratio of the blackbody surface area to the area of the sphere on which the observer rests. Its value is set as a function of blackbody temperature T and TPV system efficiency η.

The dilution factor *f*

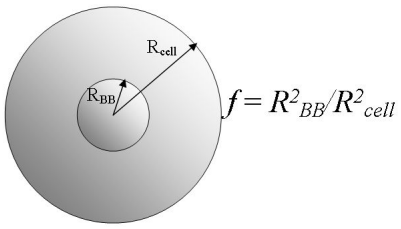

Figure 4.1: Illustration of the dilution factor f, showing the ratio of blackbody (BB) to cell surface areas

f effectively sets the distance between the cells and the blackbody surface.
For $f = \frac{R_{sun}^2}{R_{sun-earth}^2} \approx \frac{1}{46300}$, and the sun approximated as a blackbody at 5800 K, the solar constant of ~ 0.1 W/cm^2 is obtained. For the first pass analysis of the system (section 5.2), the dilution factor was set to ensure a constant 1 W/cm^2 incident power density for all blackbody temperatures. This power density was chosen in order to remove transport

resistive losses as a major factor for the first pass analysis. 1 W/cm^2 represents the lower range of actual TPV power densities. For the analysis of conventional and sliver cells in TPV systems (sections (5.7) and (5.8)), f was optimised for each cell thickness and blackbody temperature. In practice is this achieved by adjusting R - the distance between the cells and the blackbody. The optimisation involved finding the value of f for which the TPV efficiency was a maximum for each cell thickness and blackbody temperature. The code used to achieve this is presented in Appendix A.

TPV efficiency is defined as the generated electrical power output divided by the power required to keep the blackbody at its operating temperature.

$$\eta_{TPV} = \frac{P_{electrical}}{P_{radiated} - P_{returned}} \tag{4.2}$$

This equation presents the essential feature of TPV systems; the denominator is not $P_{radiated}$, but $P_{radiated} - P_{returned}$. This is due to the recycling of photons not absorbed by the cell or mirror, being returned back to the emitter. We assume here that convective/conductive losses of the TPV system are small. In sections (5.7) and (5.8) it is shown that photon recycling is a significant consideration for TPV systems. At maximum TPV efficiency, more than 60 % of the radiated energy is returned to the emitter; the value remains above 40 % across the whole range of investigated parameters.

The total input power required for the TPV system is the energy difference needed to keep the blackbody at temperature.

Spectrum generation

The TPV emitter spectrum was generated from $\lambda = 100\,\text{nm}$ to $\lambda = 1.67 \times 10^4\,\text{nm}$ with an interval size of 10 nm. The upper limit of wavelength was set at 16.5 μm to ensure the energy collected by the model was within 1 % of the total analytical energy output σT^4, with σ the Stefan-Boltzmann constant. This can be seen in figure (4.2).

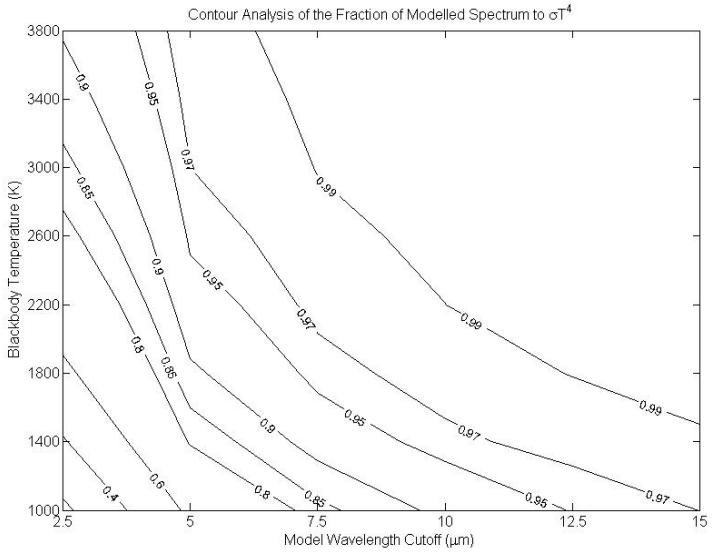

Figure 4.2: To collect more than 99 % of the spectrum at low blackbody temperatures, the cutoff wavelength must be in the tens of micrometers.

Integration within the model was performed to first order through summation of the power density over all wavelengths, multiplied by the interval size. This method has an associated uncertainty discussed further in section (4.12).

The lower wavelength limit was set at 100 nm. This was similarly to ensure maximum collection of the spectrum, with the additional limit that energy density at wavelengths shorter than 100 nm was negligibly low.

The energy spectrum was then converted to a photon density spectrum with units of photons/(s.cm^2.m) through division by a factor of $\frac{hc}{\lambda}$ as seen by:

$$N_{BB}(\lambda) = \frac{P_{BB}(\lambda)}{(\frac{hc}{\lambda})} \tag{4.3}$$

Having generated the spectrum, the path of photons through the system can now be considered.

What follows here is a presentation of each photon event moving through the cell (figure (4.3)). The path of light through the system was modelled in one dimension. The resistive losses and efficiencies were subsequently modelled using all three dimensions of the cell.

Model schematic

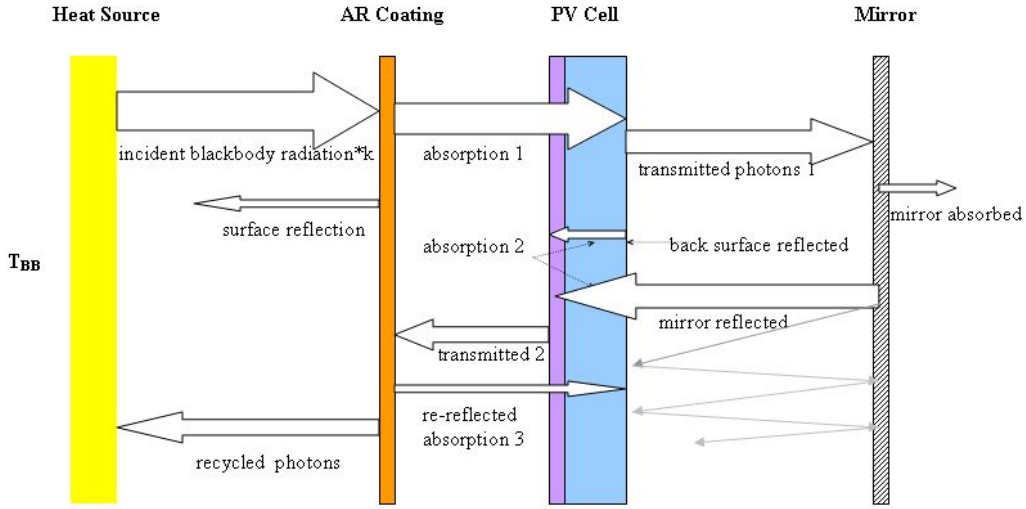

Figure 4.3: Schematic diagram of the TPV computational model.

First, the spectrum was multiplied by a flat, wavelength-independent loss k, representing geometrical non-reflected losses between the light source and the cells. k was a scalable factor taking into account gaps between cells and absorption from metal fingers and contacts.

From here, the reflectivity of the cell surface was modelled. Antireflection (AR) data $R(\lambda)$ was entered (see section (4.11)) and the number of photons reflected from the surface, N_{SR}, was calculated:

$$N_{SR}(\lambda) = kN_{BB}(\lambda)R(\lambda) \tag{4.4}$$

After the AR surface, light is incident on the cell material and absorption was next calculated. Absorption data for the material was entered (section (4.8)) and the number of

absorbed photons from this first pass, N_{abs1}, was determined:

$$N_{abs1}(\lambda) = \Big(kN_{BB}(\lambda) - N_{SR}(\lambda)\Big)\Big(1 - e^{-\alpha(\lambda)x}\Big) \tag{4.5}$$

Here x is the optical thickness of the cell and $\alpha(\lambda)$ the absorption coefficient of the cell material (figure (4.7)).

The optical thickness of the cell is equal to the physical thickness multiplied by a scalable factor relating to the degree of texturing of the cell surface. It ranges in from one, for no texturing, to a value of 50 for a perfect Lambertian surface for silicon [46]. It is not obvious whether texturing would be beneficial for TPV systems. Including texturing would increase the optical thickness of the cell allowing for greater absorption, but simultaneously reduce the number of recycled photons returned to the emitter by increasing free-carrier absorption. The factor is included for the possible future study of texturing; for the study of optimum cell thickness in this model, the texturing factor is set to one.

Following the calculation of photons absorbed by the cell from the first path of light, the corresponding short-circuit current can be calculated:

$$J_{sc1} = q(IQE)\int_{\lambda_{min}}^{\lambda_{bg}} N_{abs1}(\lambda)d\lambda \tag{4.6}$$

Here q is the electron charge, λ_{bg} the bandgap wavelength and IQE the internal quantum efficiency of the cell; the efficiency with which photon-generated electron-hole pairs are collected by the p-n junction. IQE depends on the minority carrier lifetimes in the cell material. For the first pass examination, IQE was set at 100 %. For the simulation of sliver and conventional cells IQE was set at 99 % as a result of the optimisation of bulk and emitter resistivities (section (4.5.1)).

Having passed through the cell once, the next photon events considered were reflection from the back surface of the cell and reflection from the mirror. Back surface reflectivity is a function of AR coating, texturing and method of contact to the mirror. It is a small effect and absorbed into the consideration of mirror reflectivity and multiple reflections.

Mirror reflectivity coefficients $M(\lambda)$ were entered (see section (4.10)) and the number of photons reflected from the mirror surface, N_{MR}, found:

$$N_{MR}(\lambda) = \Big(kN_{BB}(\lambda) - N_{SR}(\lambda) - N_{abs1}(\lambda)\Big)M(\lambda) \tag{4.7}$$

After reflection from the mirror surface, the photons are again incident on the back-surface of the cell. A percentage of these photons will be reflected from the cell surface - and then again be incident on the mirror. This process will continue until either the photon enters the cell or is absorbed by the mirror. Approximating the mirror reflectivity at a constant, wavelength independent $R_M = 0.98$ and the reflection of the cell surface to be a constant, wavelength independent, weighted R_w for the particular material, we can model the higher-bounce absorptions.

For silicon, with $R_w = 0.3$:

$$\begin{aligned} N_{MirrorAbs\infty} &= \Big(1 - R_M\Big)\Big(1 + (R_M R_w) + (R_M R_w)^2 + (R_M R_w)^3 + \dots \\ &= 0.02\Big(1 + (0.98 \times 0.3) + (0.98 \times 0.3)^2 + (0.98 \times 0.3)^3 + \dots \\ &= a\sum_{n=0}^{\infty} r^n \quad \text{where } a = 0.02, \quad r = 0.98 \times 0.3 \\ &= \frac{a}{1-r} \quad \text{with} \quad |r| < 1 \\ &\approx 0.028 \end{aligned} \tag{4.8}$$

That is, after the first reflection of light is considered, approximately 0.8 % of the initially incident light is additionally absorbed in the mirror from all subsequent reflections, with the remaining 99.2 % absorbed by the silicon. Equivalently, we can approximate this as the mirror absorbing 0.8% more of the incident light in the first pass. This is the method chosen and the reflectivity coefficients of the mirror were multiplied a factor $f_{MR\infty} = 0.992$. Hence we have the total number of photons reflected from the mirror and reentering the cell N_{MR}:

$$N_{MR}(\lambda) = \Big(kN_{BB}(\lambda) - N_{SR}(\lambda) - N_{abs1}(\lambda)\Big) b f_{MR\infty} M(\lambda) \tag{4.9}$$

Equivalently, we have the number of photons absorbed by the mirror:

$$N_{Mabs}(\lambda) = \Big(kN_{BB}(\lambda) - N_{SR}(\lambda) - N_{abs1}(\lambda)\Big)\Big(1 - bM(\lambda) f_{MR\infty}\Big) \tag{4.10}$$

With photons reentering the cell, we can calculate the absorption of the cell for the second pass of light.

$$N_{abs2}(\lambda) = \Big(kN_{BB}(\lambda) - N_{SR}(\lambda) - N_{abs1}(\lambda) - N_{Mabs}(\lambda)\Big)\Big(1 - e^{-\alpha(\lambda)x}\Big) \tag{4.11}$$

Again, photons will be internally reflected from the Cell-ARCoating interface. The number of photons absorbed from this third pass through the cell is the number of photons *transmitted* through the cell for the second time, multiplied by the reflection at the top surface, multiplied by the absorption factor:

$$N_{abs3}(\lambda) = \Big(kN_{BB}(\lambda) - N_{SR}(\lambda) - N_{abs1}(\lambda) - N_{Mabs}(\lambda)\Big)\Big(e^{-\alpha(\lambda)x}\Big) R(\lambda)\Big(1 - e^{-\alpha(\lambda)x}\Big) \tag{4.12}$$

Higher order reflections and absorptions are neglected here, and the total absorption contributing to short-circuit current density is found to be $N_{abs1} + N_{abs2} + N_{abs3}$.

It is assumed that all photons not absorbed from the third pass through the cell, are returned to the emitter:

$$N_{returned}(\lambda) = kN_{BB}(\lambda) - N_{abs1}(\lambda) - N_{Mabs}(\lambda) - N_{abs2}(\lambda) - N_{abs3}(\lambda) + N_{SR}(\lambda) \tag{4.13}$$

The energy returned to the emitter per second is then:

$$E_{returned} = \int_{\lambda_{min}}^{\lambda_{max}} \frac{hc}{\lambda} N_{returned}(\lambda) d\lambda \tag{4.14}$$

This is the complete photon cycle of the TPV system. From here the cells characteristics are calculated.

4.3 Cell characteristics

The intrinsic cell performance characteristics of the solar cell equation (equation (2.1)) are the reverse saturation current density J_0 , short-circuit current density J_{sc} and open-circuit voltage V_{oc}. In addition there is the ideal fill factor FF_0; the measure of the 'squareness' of the I-V curve for a cell with ideality factor of 1 (discussed below). The final fill factor FF is the ratio of the maximum power (mp) to the product of $V_{oc}J_{sc}$:

$$FF = \frac{V_{mp}J_{sc}}{V_{oc}J_{sc}} \quad \text{such that:} \qquad \text{Electrical Output } = FFV_{oc}J_{sc}$$

This section discusses each of the the cell performance characteristics.

Dark current density

First we have the dark current of the cell J_0. It is comprised:

$$J_0 = J_{0_S} + J_{0_B} + J_{0_E} \tag{4.15}$$

J_{0_S} is the surface recombination current density and is dependent on the level of surface passivation of the material. Very good surface passivation was assumed for the cells in this study. J_{0_S} was set at the lower limit of recombination that, neglecting all other recombination, must be present to limit sliver cell V_{oc} to $700\,mV$. An open-circuit voltage of 700 mV represents an excellent, and achievable, surface passivation. The corresponding value of J_{0_S} was found to be $4.8 \times 10^{-14}\,\mathrm{A/cm^2}$.

Surface recombinations near the metal-contacts of both sliver and conventional cells are neglected due to the contact regions being heavily doped. They also comprise a small fraction of cell surface area. Outer-end edge surface recombinations are similarly considered negligible.

J_{0_B} and J_{0_E}, the bulk and emitter recombination terms, are dependent on minority carrier lifetimes and diffusivities, surface recombination velocities, doping densities, and thicknesses of the base and emitter regions. For good choice of device design, J_{0_E} turns out to be negligible, this was validated using PC1D simulations.

The expression for bulk recombination is given:

$$J_{0_B} = \frac{qD_e n_i^2}{L_e N_A} F_p \tag{4.16}$$

Where D ($\mathrm{cm^2/s}$) and L (cm) are the carrier diffusivities and diffusion lengths, n_i^2 is the intrinsic carrier concentration ($\mathrm{cm^{-6}}$), N_A is the acceptor density ($\mathrm{cm^{-3}}$), and the full expression for F_p is:

$$F_p = \frac{S_e \cosh(\frac{W_p}{L_e}) + \frac{D_e}{L_e}\sinh(\frac{W_p}{L_e})}{\frac{D_e}{L_e}\cosh(\frac{W_p}{L_e}) + S_e \sinh(\frac{W_p}{L_e})}$$

S_e is the surface recombination velocity (cm/s) of the electrons, for this study is set to zero since we are assuming excellent surface passivation. W_p is the thicknesses (cm) of the bulk region [47].

There is an additional junction recombination term J_{0_J} which is neglected since it is an $n = 2$ process. This n is known as the ideality factor; for low currents $n = 2$ processes are significant, at high current $n = 1$ processes dominate, reference [47] discusses this in more detail. Due to the high currents present in TPV cells, the ideality factor is set to one and J_{0_J} is set to zero.

The final J_0 is then given:

$$J_0 = J_{0_S} + \frac{qn_i^2 D_e^2}{N_A L_e^2} \tanh(\frac{W_p}{L_e}) \tag{4.17}$$

These parameters were set for each cell material and type. They were calculated using PC1D, and are presented and discussed in section (4.5).

Short-circuit current density

Next we calculate the short-circuit current density. From the absorption of photons with $\lambda < \lambda_{bg}$:

$$J_{sc} = q(IQE) \int_{\lambda_{min}}^{\lambda_{bg}} \Big(N_{abs1}(\lambda) + N_{abs2}(\lambda) + N_{abs3}(\lambda) \Big) d\lambda \tag{4.18}$$

Open-circuit voltage

From J_{sc} and J_0, the open-circuit voltage V_{oc} can be calculated:

$$V_{oc} = \frac{kT}{q} \ln(\frac{J_{sc}}{J_0} + 1) - \kappa_v (T_{cell} - T_0) \tag{4.19}$$

Here, κ_v is the voltage temperature coefficient of the cell discussed in section (4.9).

Ideal fill factor

From V_{oc} the ideal fill factor FF_0 for silicon is calculated with the empirical expression [47]:

$$FF_0 = \frac{v_{oc} - \ln(v_{oc}) + 0.72}{v_{oc} + 1} \tag{4.20}$$

This fill factor does not yet include any resistance losses, which is the next stage of the modelling process.

4.4 Resistance losses

Through a consideration of resistance losses the final fill factor FF is obtained. FF depends upon the different power losses within the cell. The two components are parasitic shunt resistance losses and series resistances. Shunt resistances are largely dependent on the quality of cell fabrication. It is relatively easy to fabricate cells with high shunt resistance, and as a result shunt resistance losses are neglected. The main resistance loss for TPV cells is series resistance.

Series resistance

Series resistances are the natural ohmic resistances present for conduction through any material (excluding superconductors). In photovoltaic cells, they arise mainly from majority carrier current flow to cell contacts in both the emitter and bulk regions. Ohmic resistances both near and within the metal contacts also contribute to to series resistance, but can be minimised with good cell design [16]. Contact resistance was not considered for this project.

Carrier transport resistance power losses within the emitter and bulk regions are found through: $P_{loss} = \int_0^x I^2 dR$, where x is the distance charge carriers must travel. Now

$R = \frac{\rho x}{Area}$, hence $dR = \frac{\rho dx}{Area}$. Here, ρ is the resistivity of the material with units of (Ω.cm). The area is the cross-sectional area through which the carriers travel.

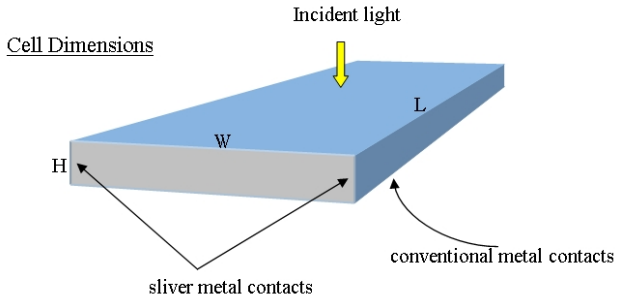

Figure 4.4: Cell Dimension labels

4.4.1 Conventional cell resistance

For conventional back-contact cells the charge carriers are transported vertically through the cell (figure (4.4)). Most photon absorption occurs relatively near the upper surface. dR for conventional cells is $\frac{\rho dH}{WL}$, and the power loss can be calculated:

$$\begin{aligned} I_{cellmp} &= WLJ_{mp} \\ P_{conventional\ loss} &= \int_0^H (WLJ_{mp})^2 \frac{\rho}{WL} dH' \\ &= WL\rho H J_{mp}^2 \end{aligned} \tag{4.21}$$

The percentage of power loss due to this resistance ($P_{conventional\ loss}\%$) for conventional cells is then found:

$$\begin{aligned} P_{conventional\ loss}\% &= \frac{P_{loss}}{P_{mp}} \\ &= \frac{WL\rho H J_{mp}^2}{WLJ_{mp}V_{mp}} \\ &= \frac{\rho H J_{mp}}{V_{mp}} \end{aligned} \tag{4.22}$$

To model $P_{loss}\%$, $\frac{J_{mp}}{V_{mp}}$ was approximated to $\frac{J_{sc}}{V_{oc}}$. In addition, for conventional cells, the resistive losses in the emitter were neglected due to the very small emitter thickness of 1.2 μm.
There are two things to note about the resistive power loss for conventional cells. The first is that the loss is linearly proportional to current density, and the second is that losses are proportional to cell thickness.

4.4.2 Sliver cell resistances

Sliver cells have their metal contacts at the edges of the cell. This results in a significantly different resistance geometry. Instead of charge carriers being transported vertically through the cell, they are transported horizontally between the edges. dR then becomes $\frac{\rho dW}{LH}$ such that we obtain:

$$\begin{aligned} I_{cellmp} &= WLJ_{mp} \\ P_{sliver\ loss} &= \int_0^W (WLJ_{mp})^2 \frac{\rho}{LH} dW' \\ &= \frac{L\rho W^3 J_{mp}^2}{3H} \quad \text{and equivalently for the emitter with} \quad R_\square = \frac{\rho}{h} \end{aligned} \tag{4.23}$$

For the emitter resistance, h is the thickness of the emitter region as opposed to H the thickness of the bulk. Emitter thicknesses are typically of the order of a few microns, sliver emitter thicknesses are $\sim 1.2\,\mu$m. $R_\square$ is the sheet resistance of the emitter with units of ohms. $R_\square$ is the resistivity per unit thickness, and hence the units are referred to as ohms per square ($\Omega/\square$).
The $P_{sliver\ loss}\%$ is then found for the bulk:

$$\begin{aligned} P_{sliver\ loss}\% &= \frac{P_{loss}}{P_{mp}} \\ &= \frac{L\rho W^3 J_{mp}^2}{3HLWJ_{mp}V_{mp}} \\ &= \frac{\rho W^2 J_{mp}}{3HV_{mp}} \end{aligned} \tag{4.24}$$

With an equivalent expression for the emitter with $R_\square = \frac{\rho}{h}$.

These expressions are significantly different to conventional cells for two reasons. Firstly, resistive losses vary as the *square* of cell width. Secondly, resistive loss is inversely proportional to cell thickness.

Final fill factor

The resistive power losses are calculated for both the base and the emitter, giving the final fill factor (FF):

$$FF = (1 - \frac{P_{baseloss}}{P_{mp}}) \cdot (1 - \frac{P_{emitterloss}}{P_{mp}}) \cdot FF_{sh} \cdot FF_0 \tag{4.25}$$

Efficiencies

The electrical output of the cell and the efficiency of the TPV system as a whole can now be calculated:

$$\text{Electrical output} = FFV_{oc}J_{sc}$$

The TPV system efficiency is then:

$$\begin{aligned} \text{TPV efficiency} &= \frac{\text{Electrical power output}}{\text{Power blackbody - Power returned}} \\ &= \frac{FFV_{oc}J_{sc}}{\int_{\lambda_{min}}^{\lambda_{max}} (P_{BB}(\lambda) - P_{returned}(\lambda))d\lambda} \end{aligned} \tag{4.26}$$

Some TPV researchers in the literature suggest calculating TPV efficiency as the ratio of electrical power output to the power absorbed by the cell. This gives an indication of cell performance, but neglects optical losses and the absorption of the mirror. For this reason, the above calculation of equation (4.26) was used.

4.5 Material resistivities

Cell performance and series resistance losses are sensitively dependent on material resistivities and minority carrier diffusion lengths. Resistivity is calculated for the p-type base: $\rho = \frac{1}{q\mu_h N_A}$ where μ_h and N_A are the hole mobility and doping density, respectively. For the emitter: $R_\square = \frac{\rho}{H}$. The base is chosen to be p-type and the emitter n-type to follow the convention for both sliver cells and the majority of conventional cells, GaSb cells are also made with this structure [39]. While opposite doping still forms a photovoltaic cell, p-type is chosen for the bulk for reasons of manufacturability and to utilise the higher mobility of electrons.

The choice of material resistivity is a trade off between internal quantum efficiency and resistive losses. Higher resistivity results in larger diffusion lengths which returns higher internal quantum efficiency (IQE). However increasing material resistivity also increases series resistance.

To find the balance of these two processes, and to find the optimal resistivities for each cell thickness in the range 10 - 1000 μm, detailed semiconductor device modelling was undertaken.

4.5.1 Bulk resistivity

For each silicon bulk resistivity, the corresponding achievable minority carrier diffusion lengths are well established. To find the values of bulk resistivity that ensured high IQE for each cell thickness, the device modelling program PC1D was used.

Nearly unity IQE is desirable since this maximises efficiency and hence power output by collecting all charge carrier pairs that were created. Different ratios of L_d to W were investigated and the value of IQE was determined by the ratio of collected J_{sc} to the value of J_{sc} obtained when the diffusion length was set at the Auger recombination limit ie. the maximum possible value [47].

The investigation was done for two cell thicknesses and resistivities, across a range of temperatures with incident power density normalised to 1 W/cm^2. The emitter sheet resistance was set to 80 $\Omega/\square$, with emitter thickness of 1.2 μm.

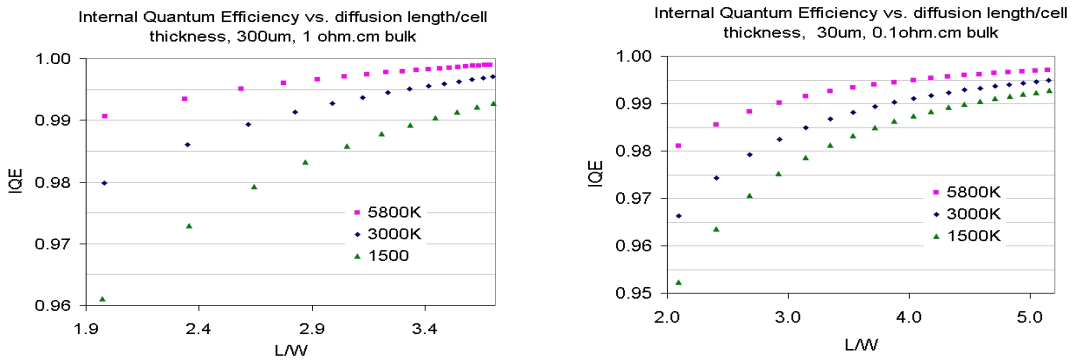

(a) **(b)**

Figure 4.5: (a) IQE analysis for a 300 μm, 1 Ω.cm cell, (b) IQE analysis for a 30 μm, 0.1 Ω.cm cell. It is observed that for thin cells and low blackbody temperatures, $\frac{L}{W}$ must be > 4.5 to ensure IQE $> 99\,\%$.

As a result of the above analysis, $\frac{L}{W}$ was kept above 5 to ensure IQE remained above 99 % for all cell thicknesses and blackbody temperatures.

4.5.2 Emitter resistivity

For the emitter resistivity, an initial value of $80\,\Omega/\square$ was used. This is a typical value of emitter sheet resistance for silicon solar cells. In the analysis of sliver cells in TPV systems, it was found that emitter series resistance was a limiting factor for performance; emitter resistance losses were approximately 4 %. It was then decided to examine optimal emitter resistivity in a similar manner to bulk resistivity.

PC1D was used to simulate a cell $50\,\mu$m thick, $0.1\,\Omega.cm$ bulk with Auger recombination limit diffusion length under different blackbody temperatures normalised to have $1\,W/cm^2$ power density; this is representative of the lower end of TPV power densities. The emitter depth was $1.2\,\mu$m with a gaussian profile, and different emitter sheet resistances were analysed. This corresponds to different doping doses.

IQE was calculated by the ratio of collected J_{sc} to the J_{sc} found for an emitter sheet resistance of $200\,\Omega/\square$, for which negligible emitter recombination occurs.

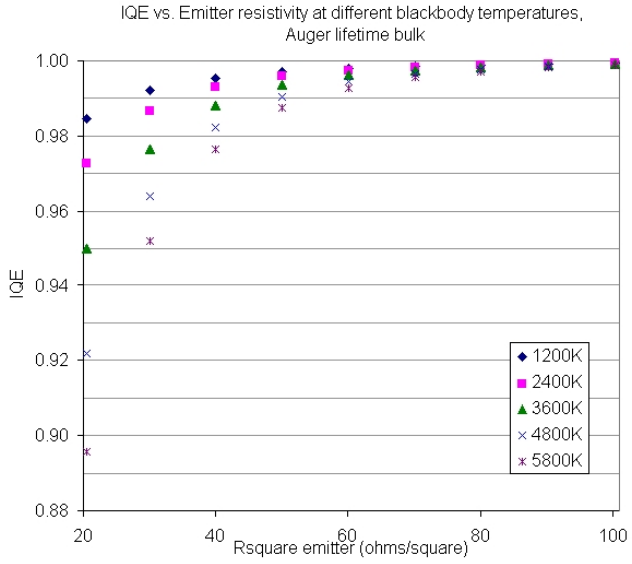

Figure 4.6: For TPV temperatures it is observed that IQE is $\approx 99\,\%$ for $R/\square = 40\,\Omega/\square$

From figure 4.6 it is observed that halving the sheet resistance from $80\,\Omega/\square$ to $40\,\Omega/\square$ results in an IQE loss of only 1 % . Since emitter resistance losses were $\sim$ 4 %, and halving the sheet resistance from $80\,\Omega/\square$ to $40\,\Omega/\square$ halves emitter resistance it was found favourable to reduce the emitter sheet resistance to $40\,\Omega/\square$ and set IQE = 99 % for a resulting net gain of $\sim$ 2 % efficiency.

4.6 Material properties

Optimal bulk and emitter dopings and corresponding values obtained from PC1D are presented in table below:.

Bulk Resistivity (Ω.cm)	Cell Thickness (μm)	Diffusion Length (cm)	Diffusivity (cm^2/s)	N_a bulk (cm^{-3})	N_d emitter (cm^{-3})
0.1	$10-28$	0.015	13.36	2.34×10^{17}	3.13×10^{19}
0.2	$29-65$	0.035	17.59	9.58×10^{16}	3.46×10^{19}
0.5	$66-153$	0.075	23.21	3.26×10^{16}	4.21×10^{19}
1.0	$154-1000$	0.1	26.88	1.51×10^{16}	4.21×10^{19}

Table 4.1: Material parameters for silicon conventional and sliver cells in the TPV model. The diffusion lengths were set according to [27]

In addition emitter junction depth was set at $1.2\,\mu$m, and intrinsic carrier concentration (n_i^2) was set to $1\times10^{20}\,cm^{-6}$, the accepted value for silicon at room temperature.

The limited number of the values of resistivity were a source of uncertainty; the resulting discontinuities in cell performance can be noticed in the figures of sections (5.7) and (5.8). In addition, the highest resistivity modelled of $1\,\Omega$.cm does not ensure near unity IQE for the higher cell thicknesses, this effect is considered in section (4.12).

4.7 Cell parameters

Sliver cell and conventional cell parameters were included as follows.

Sliver cells

Cell width =0.3 cm
Cell length =10 cm
Cell flat optical loss =1 %
Emitter thickness = $2*1.2\,\mu$m
$J_{0_S} = 4.8\times10^{-14}\,A/cm^2$
Rear surface weighted reflectivity =0.03
V_{oc} cell temperature coefficient =2.1 mV/K
Fill factor cell temperature coeff: =0.2 %/K, modelled to (0.002× FF_0)/K

The width is a practical minimum width of slivers, limited by silicon wafer thickness [27]. The flat loss of 1 % is included to model the gaps between sliver cells due to the contacts at the edges [27]. Effective emitter thickness and surface recombination are doubled as a result of sliver cells being bifacial. The rear surface weighted reflectivity value is a result of the sliver cell fabrication process; any anti-reflection coating for sliver cells will be applied to both faces of the cell (figure (2.5)). The cell temperature coefficients are discussed in section (4.9).

Conventional cells

Cell flat optical loss 0 %
Emitter thickness =1.2 μm
$J_{0_S} = 2.4 \times 10^{-14}$ A/cm^2
Rear surface weighted reflectivity =0.3
V_{oc} cell temperature coefficient =2.0 mV/K
Fill factor cell temperature coefficient =0.2 %/K

With vertical carrier transport in conventional cells, cell width and length do not need to be specified. J_{0_S} is set for surface recombination at one surface. Rear surface reflectivity is set to the weighted reflectance for silicon since no anti-reflectance coating would usually be applied to the backsurface of conventional cells. Flat optical losses are set to zero since back contact cells can be butted up very close to each other and have no front contacts from which parasitic reflection can occur. These assumptions are of dubious validity for the outer parameter ranges of TPV operaton. For large values of current density, back-contacts would need to increase in order to control contact resistance. This would increase the value of flat optical loss for conventional cells, and is discussed further in section (5.9). In addition, as cell thickness decreases, surface recombination starts to occur at both surfaces and the corresponding value of J_{0_S} increases to be comparable to that of sliver cells. Excellent contact design and surface passivation are assumed for conventional cells, however the effects of the above assumptions is significant low cell thicknesses. It is further discussed in the uncertainty section (section (4.12)).

4.8 Absorption data

Silicon absorption data was taken from Green (1987) [48] from the presented range 100 nm to 1240 nm (figure(4.7)a). Beyond this, in the range 1240 nm to 1450 nm, the absorption coefficient was taken from Adachi (1999) [18] (figure(4.7)b).

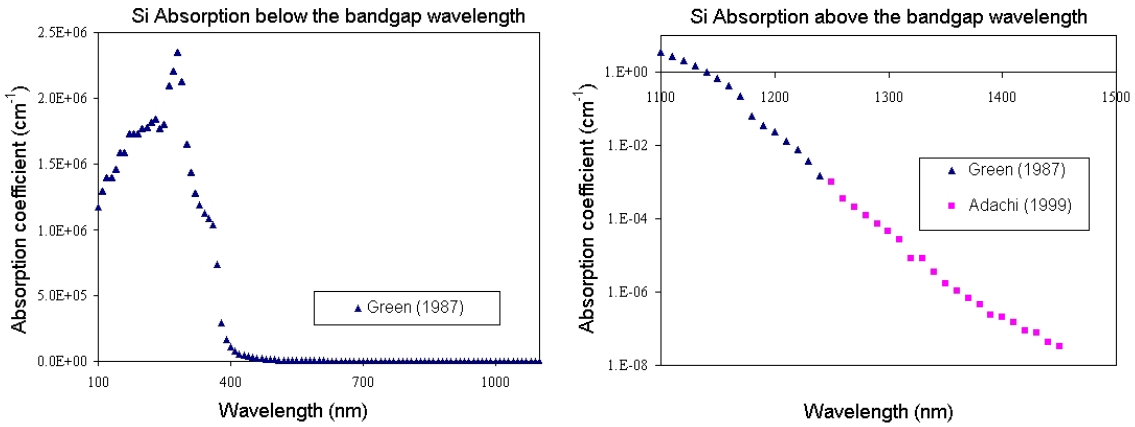

(a) **(b)**

Figure 4.7: (a) The absorption coefficient structure is of high absorption for short-wavelengths decreasing towards the bandgap wavelength of 1100 nm, (b) Log-linear plot of the absorption coefficients; the linear trend in the figure represents exponential decrease in absorption for wavelengths beyond the bandgap

The exponential fit for the absorption coefficient α for wavelengths longer than the bandgap wavelength is:

$$\alpha = 3 \times 10^{28} e^{-(6\times10^7)\lambda} \tag{4.27}$$

Absorption coefficients for λ >1450 nm were modelled to follow this fit.

For comparison the absorption coefficients of Gallium Antimonide are also presented in figure (4.8). To note is the similar absorption structure to silicon; large absorption for

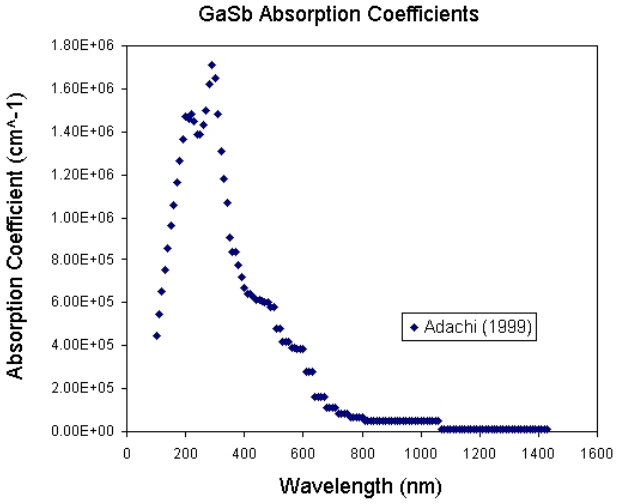

Figure 4.8: Absorption data of gallium antimonide. The bandgap wavelength is 1720 nm [18, 42]. A similar absorption structure to silicon is observed.

short-wavelengths, decreasing exponentially for longer wavelengths.

4.9 Cell temperature

Cell temperature is a key consideration for TPV systems [42, 49, 50]. Proximity to objects with tempterature T >1000 K requires an excellent cooling system. For the first-pass analysis of cells in TPV systems (section (5.2)), cell temperature was set to 298 K, room temperature. For the simulation of conventional and sliver cells in TPV systems, cell temperature was set to 20°C above ambient(318 K). This was used to represent an excellent cooling system. In practice, acceptable cell temperature is set by the trade-off between cell performance and cooling system energy requirements and cost. $20°C$ above ambient represents an excellent, achievable, cooling system.

Increasing cell temperature increases intrinsic carrier concentration (n_i^2) and carrier mobilities. Higher cell temperatures also increases absorption coefficients, and lowers the bandgap of the semiconductor. The main result of these effects on cell performance is a lowering of open-circuit voltage [51], which in turn reduces the electrical power output. Increasing cell temperature also decreases the fill factor, and slightly increases short-circuit current density by a small amount due to increased carrier mobilities.

The effects of cell temperature were modelled through the inclusion of temperature coefficients for V_{oc} and FF. With IQE > 99%, the J_{sc} coefficients were set to zero.

Sliver V_{oc} temperature coefficients were taken from the work by Everett *et al.* (2004) [51]. Sliver FF and conventional cells FF and V_{oc} temperature coefficients were taken from the specifications of a high-quality monocrystalline silicon solar cell manufactured

by Spectrolab [52].

The effects of cell temperature are examined in section (5.5).

4.10 Mirror reflectivity

The back surface mirror of a TPV system is another component that was observed to have a strong effect on efficiency; photons absorbed by the mirror are lost both to the cell and to the emitter. Consistent with the approach of modelling excellent, but achievable system parameters, mirror reflectivity values (figure (4.9)) were obtained from an infrared telescope built by the National Astronomical Observatory of Japan [53]; this represents the upper limit of achievable reflectance.

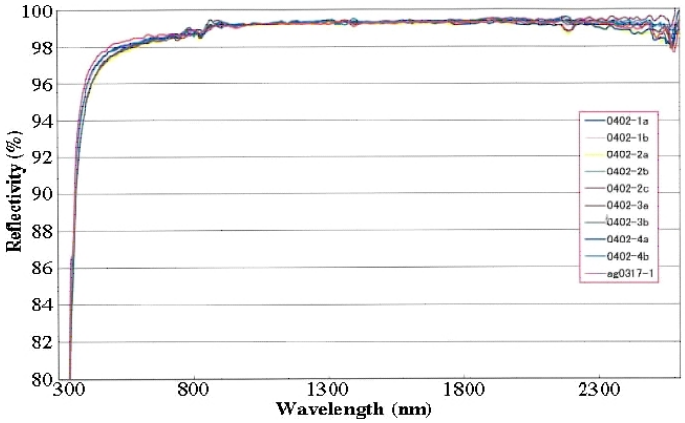

Figure 4.9: Mirror reflectivity data of an infrared telescope built by the National Astronomical Observatory of Japan [53]. The reflectance data represents the upper limit of achievable reflectivity.

Low reflectivity is observed for short wavelengths in figure (4.9); this is not so much of a problem for a mirror in a TPV system which is behind photovoltaic cells that absorb strongly in the blue end of the spectrum. For $\lambda > 2600\,\text{nm}$, reflectivity values set at a constant 98 %.

4.11 Antireflection coating

The optimisation of antireflection (AR) coating for TPV cells is an important issue, though not a primary focus for this study. The choice of AR coating was based on finding an excellent antireflectance scheme for practical available materials.

In theory, extremely good AR coatings are possible with the use of many layers of thin films [54]. In practice, AR schemes are limited to two to three layers. AR coating is intimately linked to texturing, the passivating layer of the cell and the incident spectrum; for TPV systems photon recycling must also be considered [23, 47].

For this study a Dual Layer Antireflection Coating (DLAR) was chosen that was optimised for polished, untextured Silicon under solar radiation [55]. As seen in figure (4.10), optimisation for solar radiation performs well for the longer wavelengths present in a TPV system.

The DLAR consisted of an MgF_2 layer with d_1 =104 nm, n_1 = 1.4 and a ZnS layer with d_2 = 80 nm, n_2 =2.3. The experimental and theoretical values were presented and compared by Boufhas *et al* (1998) [55] in figure (4.10):

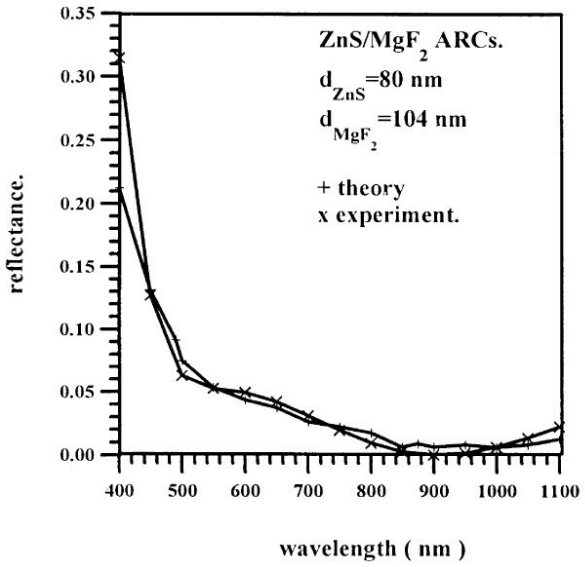

Figure 4.10: Experimental and calculated reflectance vs. wavelength of two-layer MgF_2/ZnS ARC on silicon

The experimental values in figure (4.10) were used for our model. The theory of thin film optics presented in [54] was used to extrapolate reflectance data beyond the presented data range (figure (4.11)).

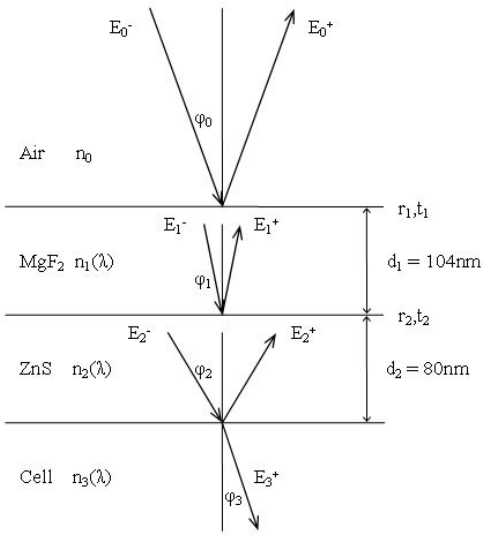

Figure 4.11: Reflection and transmission of light by two thin films. The double layer antireflectance coating consists of a thin film of magnesium flouride on top of a thin film of zinc oxide, applied to a semi-infinite silicon substrate.

$$E_0^- = \frac{r_1 + r_2 e^{-2i\delta_1} + r_3 e^{-2i(\delta_1+\delta_2)} + r_1 r_2 r_3 e^{-2i\delta_2}}{1 + r_1 r_2 e^{-2i\delta_1} + r_1 r_3 e^{-2i(\delta_1+\delta_2)} + r_2 r_3 e^{-2i\delta_2}} E_0^+ \tag{4.28}$$

$$\text{where} \qquad \delta_\alpha = \frac{2\pi}{\lambda} n_\alpha d_\alpha \cos\phi_\alpha, \qquad r_\alpha = \frac{n_{\alpha-1} - n_\alpha}{n_{\alpha-1} + n_\alpha}$$

Here, E_0^- is the amplitude of the incident electric vector and E_0^+ the amplitude of the reflected vector. δ_α and r_α are the phase changes and Fresnel coefficients, of each of the layers, respectively. The silicon layer, $\alpha = 3$, is assumed semi-infinite. The angle of incidence is set to the normal $\phi = 0$, and the expression is polarisation independent. The films were also assumed to be non-absorbing.
The final reflectivity of the surface is then given:

$$R = \left| \frac{E_0^-}{E_0^+} \right|^2 \tag{4.29}$$

4.12 Uncertainty

Uncertainty within the TPV model arose from three main areas; discretization, input data and model form error.

Discretization error

Discretization error can be quantified by the Richardson extrapolation for uniformly discretized models, presented in Rebba *et al.* (2006) "Validation and error estimation of computational models" [56].

$$\varepsilon_h = \frac{f_1 - f_2}{r^p - 1} \tag{4.30}$$

Here, f_1 and f_2 are the solutions with coarse and fine meshes respectively, $r = h_2/h_1$ is the grid refinement ratio, and the order of convergence p obtained from the relation $p = \ln(f_3 - f_2/f_2 - f_1))/\ln(r)$, with f_3 the solution obtained with the finest grid size, and $r = h_2/h_1 = h_3/h_2$.

The above analysis was undertaken for the calculation of the Planck energy density spectrum. The resulting error was found to be negligible compared to the errors from input data error and model form error.

Input data error

While the modelled cell material parameters were modelled as exact, uncertainty arose through the extrapolations of the silicon absorption coefficients, anti-reflectance coating values and mirror reflectivities. Additional error was present due to the cut off wavelength of the generated spectrum.

Wavelength cutoff error was attempted to be minimised by the analysis of figure (4.2), and extrapolation errors were attempted to be minimised through reasonable extrapolation techniques: for silicon absorption coefficients, data was extrapolated according to the exponential decrease observed for long wavelengths photons. For mirror reflectivity, reflectances for long wavelengths were held constant at the value for the longest wavelength presented in the data. And for anti-reflectance values, data was extrapolated using the optics of thin-films.

Again, these uncertainties were found to be small compared to the uncertainty arising from the TPV model form, and the process assumptions within it.

Model form

The selection of a one-dimensional linear model limits the accuracy with which device processes can be modelled. Detailed device models which solve the coupled non-linear semiconductor equations, calculate current flow and transport resistance losses through each region of the device, and then find the maximum power point. The developed TPV model instead calculated J_{sc} through the absorption of above-bandgap photons, used a pre-determined value of J_0 to calculate V_{oc}, and then used an empirical formula of FF_0 and calculated resistances to evaluate final cell performance. The calculations of the model assumed an ideality factor of 1 [47], and approximated J_{mp}/V_{mp} to J_{sc}/V_{oc}. In addition, bulk resistivity for large thicknesses was limited to 1Ω.cm leading to uncertain IQE values.

The uncertainty due to a set recombination current density can be approximately quantified. As mentioned in section (4.7) back-contact cells were modelled as having only one surface in which surface recombination can occur. This is a reasonable assumption for conventional thickness cells of ∼300 μm, but is of dubious validity for lower cell thicknesses when large relative diffusion lengths enable charge carriers to recombine at the rear surface. The surface recombination current density (J_{0_S}) for conventional cells was modelled as having half the value of J_{0_S} for sliver cells. For thin back-contact cells, J_{0_S} would be expected to be comparable with that for sliver cells, leading to a corresponding decrease in open-circuit voltage of $\sim (kT/Q)\ln(2)$. As a result, conventional cell power densities at low cell thicknesses were modelled as being approximately 2 % higher than would be expected.

To quantify the uncertainty due to the remaining assumptions of the model, the device modelling program PC1D was used. The precision of PC1D is substantially higher than the precision of knowledge about the TPV model data. PC1D was run with none of the above device process assumptions, enabling an examination of their effect on the results of the calculated TPV model. The models were found to agree excellently to within 1 % for the whole range of blackbody temperatures and incident power densities under investigation. Across the range of cell thicknesses, the models agreed very well for thicknesses $< 500\,\mu$m, but diverged slightly for larger thicknesses. This was due to the overestimation of bulk internal quantum efficiency for thick cells in the TPV model.

With the considerations of internal quantum efficiency and surface recombination density (J_{0_S}), and also with consideration of the extrapolation of TPV component parameters, the uncertainty of the TPV model is presented as ± 4 % for cell thicknesses 10 - 500 μm and ± 5 % for cell thicknesses 500 - 1000 μm. Much of the analysis for this project is done qualitatively without reference to specific efficiency values. When quantitative comparisons are made, the above uncertainty values are used.

TPV modelling for this project was carried out using the Visual Basic programming language and spreadsheets within Excel. The accuracy of the constructed model was examined with PC1D.

Chapter 5

Results and Discussion

This chapter presents the results of modelling. Firstly, in section (5.1) the validation of the TPV model is discussed. Validation was considered by modelling the same cell under normal illumination in both PC1D and the TPV model. Section (5.2) presents the initial first-pass result of the TPV model. This examination was of an ideal cell at constant incident power density, with only transport losses switched on. The simulation enabled an examination of the efficiency processes over the range of TPV temperatures and cell thicknesses. Section (5.3) examines the effect of spectral filtering on this ideal cell at constant incident power density; both above and below bandgap filtering is analyzed, enabling a more detailed examination of the effect of blue-loss, free-carrier absorption and resistive power losses. Sections (5.4) and (5.5) examine the effect flat optical losses and cell temperature, respectively, on a TPV system at constant incident power density.

After this initial analysis of the relative component effects on a TPV system at constant power density, sections (5.7) and (5.8) analyze conventional and sliver cells with incident power density optimised for each cell thickness and blackbody temperature. Within the range of parameters examined, it was found that sliver cells do not offer an advantage over conventional cells in TPV systems. Optimal cells for thermophotovoltaic systems were found to be thin back-contact cells with spectral filtering that reflected high energy photons back to the emitter. Potential fabrication processes for the manufacturing of optimal thermophotovoltaic cells are outlined.

Section (5.9) discusses the effects of heat sinking, cell shading, and cell-module circuitry for TPV systems, and considers future practical development of TPV cells.

Section (5.10) summarises the modelling results, discusses the comparison between sliver cell and conventional cell geometries, and considers the extrapolation to gallium antimonide cells in TPV systems.

5.1 Model validation

Once each modelling stage was developed as presented in Chapter 4, the model as a whole was validated. Extensive testing of the TPV model was done using PC1D; the one-dimensional cell modelling program developed at Sandia National Laboratories [17]. For each range of blackbody temperatures, cell thicknesses and power densities, TPV model results were closely compared with the results from PC1D.

PC1D numerically solves the fully coupled non-linear equations of electron transport in semiconductor materials. It is a program excellently suited for detailed modelling one dimensional solar device processes.

For comparison with PC1D, the TPV model was adjusted to measure the output of a solar cell under normal illumination without TPV geometry. The same cell parameters were entered into each modelling program and the results were compared.

The difference in the two approaches manifests itself in the calculation of internal quantum efficiency (IQE). IQE is defined as the efficiency with which electron-hole pairs are collected by the p-n junction for use in the external circuit. IQE decreases with the ratio of minority carrier diffusion length to cell thickness; this is a result of increased levels of recombination in the cell. Unlike the TPV model, PC1D does not explicitly set a constant IQE value; it is intrinsically calculated through the transport equations. For model comparison, material resistivities (and hence diffusion lengths) were set at values which ensured close to 100 % IQE. The decrease in IQE as modelled by PC1D can be seen in figures (5.2)b and (5.3).

The validation of the TPV model and comparison with PC1D can be classified into four main areas; 1) blackbody spectrum generation, 2) photon absorption 3) short-circuit current density, open-circuit voltage, and fill factor calculations, and 4) the calculation of transport resistive losses.

A selection of the PC1D and TPV model calculations are presented below. Cell characteristics were tested and compared across an extensive range of parameters. The selection presented encompasses the calculations of spectrum generation and cell absorption in figure (5.1)a, J_{sc} and V_{oc} calculations in (5.1)b, all of J_{sc}, V_{oc} and FF calculations in figures (5.2)a and (5.2)b, and all of J_{sc}, V_{oc} and FF with resistive transport losses in figure (5.2)b.

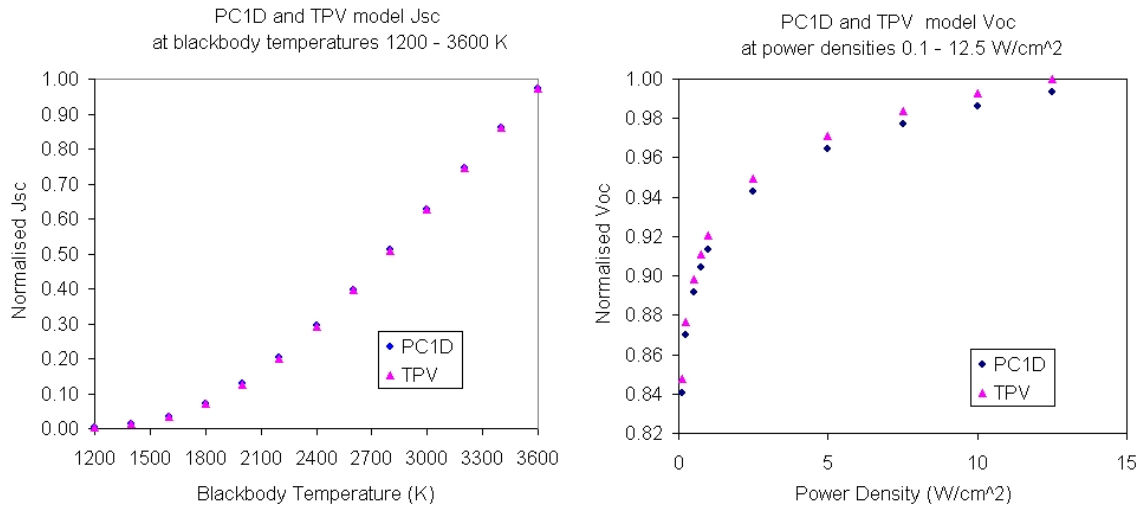

Figure 5.1: (a) Comparison of TPV model and PC1D short-circuit current densities for a wide range of blackbody temperatures. J_{sc} normalised to 14 mA, Incident power density 0.1 W/cm^2, 0.1 Ω.cm bulk, cell thickness 10 μm. Good agreement is seen across the range of blackbody temperatures. **(b)**Comparison of TPV model and PC1D open-circuit voltages for incident power densities at which TPV systems operate. Blackbody temperature 5800 K, 0.1 Ω.cm bulk, cell thickness 10 μm, Voc normalised to 815 mV. This figure examines the calculation of J_{sc} and V_{oc}. Reasonable agreement, to within 1 %, is observed between the two models across the range of power densities.

The difference in the two models can be seen for high power densities in figure (5.2)b. This is due to decreasing IQE for increasing cell thickness - an effect that the TPV model does not model directly. The difference is more clearly seen when we compare the short-circuit current density for different cell thicknesses, illustrated in figure (5.3).

The adjustment for IQE was taken into account in the TPV model by ensuring that

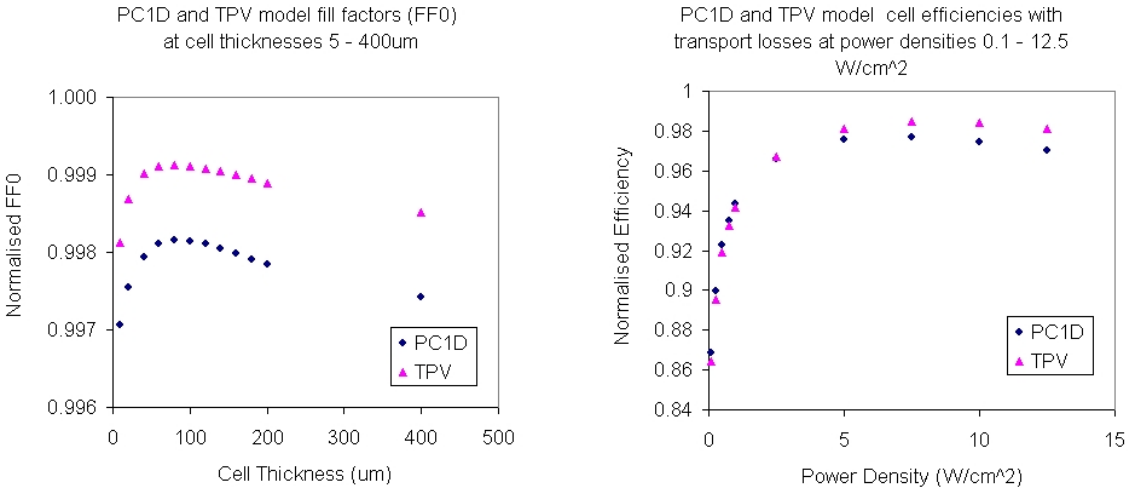

Figure 5.2: **(a)**Comparison of TPV model and PC1D Fill Factors at different cell thicknesses. Blackbody temperature 5800 K, 0.1 Ω.cm bulk, Auger limit minority carrier lifetime, FF normalised to 0.847. Good agreement, to within 0.2 %, is observed for the calculation of fill factors between the two models. **(b)**Comparison of TPV model and PC1D cell efficiencies with transport losses at TPV power densities. Blackbody temperature 5800 K, 100 μm cell thickness, 1 Ω.cm bulk, Auger limit minority carrier lifetimes, efficiency normalised to 0.243. As power densities increase, J_{sc} increases also; leading to transport resistive losses according to equation (4.22). Resistive losses have reached $\sim$ 5 % at 12.5 W/cm^2. The detachment of the two models for high thicknesses is clearly seen.

the minority carrier diffusion length remained sufficiently high to guarantee near 100% IQE (section (4.5)). This is also the case in practice when manufacturing cells.

The TPV model was also run at a blackbody temperature of 5800K and incident power density of 0.1 W/cm^2; standard solar conditions. With cell thickness of 60 μm, 0.1 Ω.cm bulk resistivity, and 80 Ω/□ emitter resistivity, the TPV model returned J_{sc} = 31.4 mA/cm^2, V_{oc} = 697 mV, FF_0 = 0.846 and an efficiency of 18.5 %. These figures correspond well to the established performance figures for fabricated sliver cells [27].

Again it is stressed that only a small sample of validation results are presented. A wide range of cell parameters were examined in both the TPV model and PC1D and found to agree.

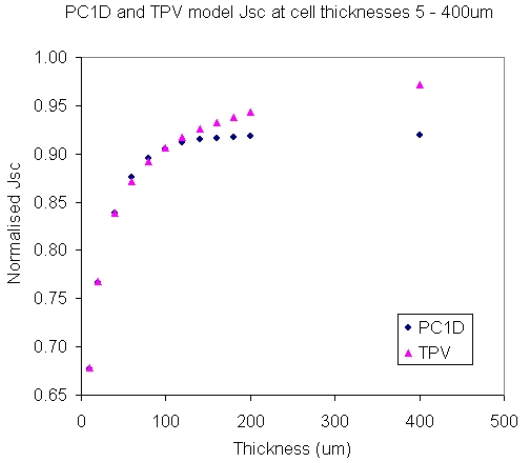

Figure 5.3: Comparison of TPV model and PC1D short-circuit current densities for different cell thicknesses. Blackbody temperature 5800 K, 0.1 W/cm^2, 0.1 Ω.cm bulk, Jsc normalised to 36 mA/cm^2. The effects of internal quantum efficiency differences are clearly observed at high cell thicknesses; this is due to bulk resistivity being set at a constant 0.1 Ω.cm. For the simulation of conventional and sliver cells in TPV systems, material resistivity was adjusted for each cell thickness to ensure IQE was greater than 99 %.

With cell resistivities set correctly the TPV model agreed with PC1D to within 1% for all J_{sc}, V_{oc} and FF calculations. It is considered a key outcome of this thesis that the constructed model simulates light absorption and J_{sc}, V_{oc}, FF and resistive loss calculations with sufficient precision to engage in an analysis of thermophotovoltaic systems.

5.2 First pass

The first use of the model was to gain a broad picture of optimal cell characteristics in thermophotovoltaic geometries. This was done by analysing an ideal cell with the incident power density of each blackbody spectrum normalised to 1 W/cm^2. The system was modelled with a perfect mirror, no parasitic optical losses and complete anti-reflection coating. This enabled the identification of the location of efficiency maxima, a further verification of the model, and an analysis of the spectral processes of the system.

The modelled idealised cell comprised of 1 Ω.cm bulk resistivity with high diffusion length of 1 mm, 80 Ω/□ emitter resistivity and 1.2 μm emitter thickness. The cell was modelled with vertical transport losses at room temperature and a constant incident power density of 1 W/cm^2. These figures were chosen to be representative of optimal TPV parameters. However, as modelled and discussed in following sections (5.7) and (5.8), both optimal cell resistivity and optimal incident power density change with blackbody temperature, cell geometry and cell thickness. For this first pass analysis there was no reflection from the cell layer, no flat optical losses and the mirror had perfect reflectivity.

Figures (5.4) and (5.5) show a clear maximum which drops on either side for both temperature and thickness.

This maximum is a result of the tradeoff between increasing efficiency due to higher current density, open-circuit voltage and output power of the cell, and decreasing efficiency due to blue-loss, free-carrier absorption and resistive transport losses. First discussed is the nature of the increase in efficiency due to increased current density and open-circuit voltage. Subsequently discussed are the three efficiency loss processes.

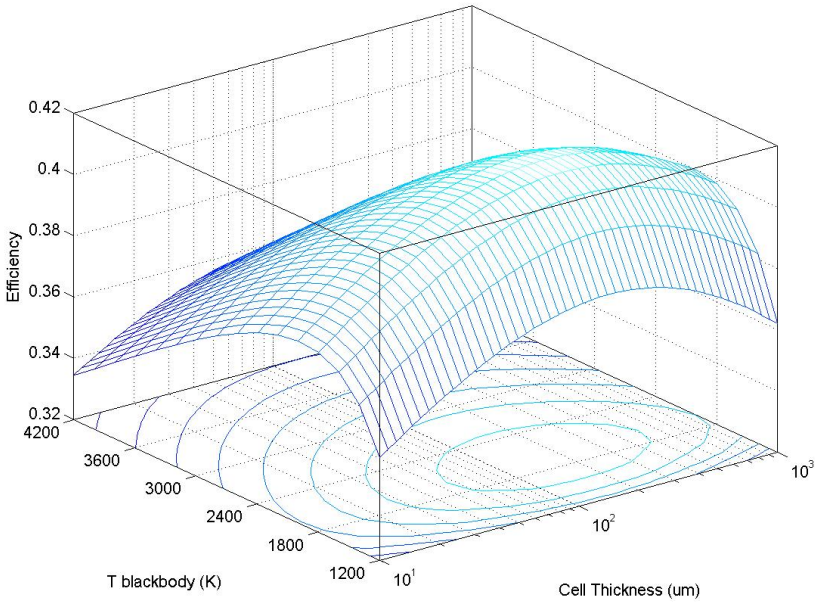

Figure 5.4: A 3-dimensional picture of optimal cell thickness and blackbody temperature with an idealised conventional cell at a constant incident power density. An efficiency maximum is seen in both blackbody temperature and cell thickness directions.

5.2.1 Electrical power output and J_{sc}

Open-circuit voltage depends logarithmically on short-circuit current density (equation (4.19)). A factor of 10 increase in short-circuit current density results in $\frac{kT}{q}\ln(10) \approx 62\,\text{mV}$ increase in open-circuit voltage. For cells operating at $\sim 600\,\text{mV}$, this represents an increase in power of $\sim 10\,\%$. Higher open-circuit voltage is the primary reason for increased efficiency at higher current densities. In ideal TPV systems, output power and efficiency increase with blackbody temperature until the theoretical maximum derived by deVos [2] and Harder and Wurfel [3] presented in section (2.4) is reached. In practical TPV systems electrical power and efficiency increase through the adjustment of incident power density until resistive losses, and to a lesser extent blue-loss and free-carrier absorptions, become appreciable. This is seen in section (5.7).

5.2.2 Resistive transport losses

Associated directly with current density is resistive transport loss. Transport losses are a result of the charge carriers being transported from the place of their generation to the cell metal contacts. In back-contact cells it is a vertical path from the top to the bottom of the cell and in sliver cells it is a horizontal path to the contacts at the edges of the cell.

As presented in section (4.4.1), the percentage of power loss due to resistive transport for conventional cells is given:

$$P_{conventional\ loss}(\%) = \frac{\rho H J_{mp}}{V_{mp}} \tag{5.1}$$

For sliver cells:

$$P_{sliver\ loss}(\%) = \frac{\rho W^2 J_{mp}}{3 H V_{mp}} \tag{5.2}$$

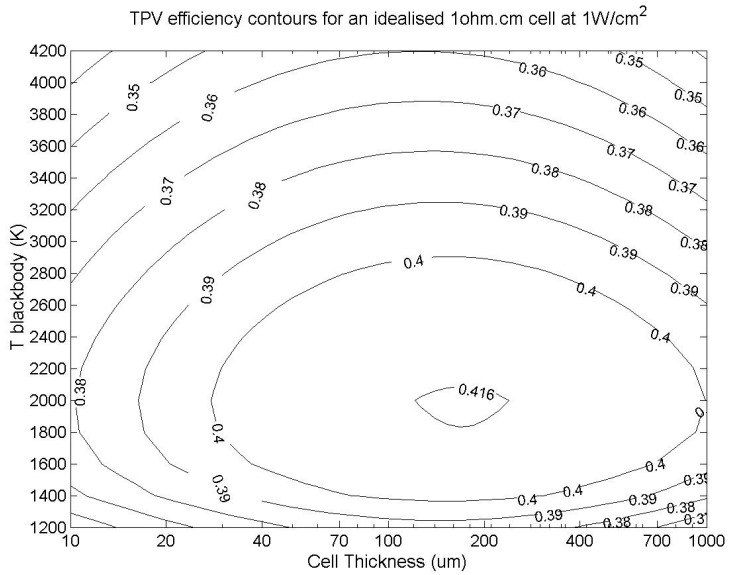

Figure 5.5: Efficiency contours as a function of thickness and blackbody temperature with an idealised conventional cell at a constant incident power density. Cell thickness is displayed with a logarithmic scale. The efficiency maximum is a balance between rising J_{sc} and V_{oc} increasing efficiency, and blue-losses, transport resistance and free-carrier absorption, decreasing efficiency.

The difference between these two formulas is the primary source of the difference in performance between sliver and conventional cells in TPV systems. Of particular importance is the W^2 factor in the sliver transport loss equation.

In the first pass simulation with incident power density normalised to $1\,\mathrm{W/cm^2}$, transport losses are removed as a major factor. This enables an examination of spectral effects on TPV efficiency.

For constant incident power densities, in figure (5.5) and in sections (5.3), (5.4) and (5.5), efficiencies are found to be only weakly dependent on cell thickness. Cell thicknesses are presented on a logarithmic scale, and the observed efficiency maxima are broad. This is not the case in sections (5.7) and (5.8), when incident power density is optimised.

With the ability to optimise incident power density for TPV systems by adjusting the distance between the cells and the emitter, transport losses are found to be the strongest loss mechanism with a significant dependance on cell thickness.

5.2.3 High-energy photon absorption losses

In TPV systems as the incident spectrum shifts to higher energies, the proportion of absorbed photons with energies higher than the bandgap energy also increases. This initially leads to an increase in efficiency since there are more photons available to generate current. However, the excess energy of higher than bandgap photons is not used by the cell, nor returned to the emitter. An electron excited by a high-energy photon rapidly thermalises to the conduction-band edge, generating heat in the process. Consequently, there is an efficiency maximum for blackbody temperature; a balance between higher temperatures generating more current and too-high temperatures resulting in wasted photon energy. This 'waste' of high-energy photons is referred to as blue-loss. Blue-loss results in decreasing TPV efficiency for increasing blackbody temperature.

Blue-loss also results in decreased efficiency for thin cells. The initial expectation was

that thin cells would lead to higher efficiencies in TPV systems. This was based on the consideration that thin cells have less free-carrier absorption than thick cells. Lower levels of free-carrier absorption allow greater proportions of sub-bandgap photons to be recycled back to the emitter, thus conserving its energy. While this is the case, an additional loss mechanism is present.

The absorption coefficient structure of silicon and most semiconductor materials (see figure (4.7) and (4.8)) gives proportionally higher absorption coefficients for the blue end of the spectrum. That is, the thinner the cell, the less the relative absorption of photons with lower energy. 'Optimal' photon absorption in an ideal TPV system is monochromatic absorption at slightly higher-than-bandgap photon energy.

As cell thickness decreases, the ratio of absorbed high-energy photons to absorbed optimal-energy photons increases. This effect leads to a reduction in TPV efficiency for decreasing cell thickness due to larger proportions of wasted photon energy. That this process is of at least the same importance as free-carrier absorption is a key finding of this project. This is further discussed in section (5.3).

5.2.4 Free-carrier absorption

Increasing cell thickness leads to greater absorption of just-higher-than-bandgap photons as outlined above. It also to leads greater absorption of sub-bandgap photons. The absorption of sub-bandgap photons is known as free-carrier absorption. In figure (4.7) free-carrier absorption is all absorption that occurs below 1.12 eV; photons with energy less than the bandgap energy. Free-carrier absorption heats the cell, does not contribute to electrical power, and reduces the amount of energy available for recycling. A trade-off between increased cell thickness leading to higher current and V_{oc}, and increased thickness leading to greater free-carrier absorption, is observed.

Similarly, as the incident spectrum is shifted to lower colour-temperatures, more sub-bandgap photons are incident on the cell leading to proportionally higher free-carrier absorption. Hence, in addition to decreased current, lower blackbody temperatures lead to decreased efficiency due to higher relative proportions of free-carrier absorption.

The two processes of blue-loss for thin cells and free-carrier absorption for thicker cells, contribute to the determination of the optimal cell thickness.

5.2.5 Summary of the first pass simulation

The ideal system simulation enabled a first pass examination of the relative importance of the different power generation and efficiency loss processes in a TPV system. A key finding is that spectral considerations do not clearly favour thin cells. Blue-loss was found to be of the same importance as free-carrier absorption, and lead to a marked decrease in efficiency for thin-cells. This was contrary to prior assumption and is discussed further in section (5.3.3).

The first pass simulation was run at a constant power density of 1 W/cm^2 in order to remove transport resistive losses as a major factor. In practice, incident power density would be adjusted by moving the cells closer or further away from the emitter to ensure that optimum efficiency and power output would be obtained in relation to resistive losses. For the simulation of conventional and sliver cells in realistic TPV systems (sections (5.7) and (5.8)), modification of incident power density was the case. Cell resistivity is another parameter that would be adjusted in realistic TPV systems according to cell thickness; the optimal values are presented in section (4.7), and were used in the conventional and sliver cell simulations in sections (5.7) and (5.8).

To gain a more detailed picture of blue-loss and free-carrier losses, spectral filtering of the cell at constant incident power density was examined. Spectral filtering is considered an important characteristic of TPV systems [13, 30], and is examined in the following section.

5.3 Spectral filtering

Spectral filtering allows control of the spectrum incident on the cell. As discussed previously in Chapter 2, spectral filtering can be achieved in four different ways; 1) through the use of a selective emitter, 2) through the use of a filter between the emitter and cell, 3) through the use of an anti-reflection coating on the cell, and 4) through the thickness of the cell allowing recycling of photons.

Each of the four alternative processes have the same goal - to ensure maximum absorption of 'ideal' photons and reduce the absorption of sub-bandgap and super-bandgap photons.

To examine the effect of spectral filtering on the determination of optimum thickness, blackbody temperature and efficiency, the emitted spectrum was filtered first for photons $E < E_g$, then next for $E > 1.42\,\mathrm{eV}$ and then subsequently for both simultaneously $1.42\,\mathrm{eV} < E < E_g$.

The energy 1.42 eV was used to simulate a gallium *arsenide* cell in a layer above the thermophotovoltaic cell. Gallium arsenide is currently being used as the first layer in multijunction concentrator solar cells and is considered a possible semiconductor material for the use of multijunction thermophotovoltaic devices.

Spectral filtering was simulated through the moderation of the blackbody spectrum. For example, to model 50 % below bandgap filtering, the blackbody radiation was multiplied by 0.5 for all wavelengths longer than the bandgap wavelength $\lambda > \lambda_g$. The filtering was done after the normalisation of incident power density to $1\,\mathrm{W/cm^2}$. This has the effect of simulating the reflection of 50 % of all photons with $\lambda > \lambda_g$ before they reach the cell surface - since reflected photons are recycled back to the emitter.

Removing the incidence on the cell of sub-bandgap photons allows the examination of the strength of free-carrier absorption (through its absence). Similarly, removing high-energy photons enables an analysis of the effect of blue-losses. Reflecting both allows a comparison of the strength of blue-loss and free-carrier absorption, and also an examination of optimum J_{sc}.

5.3.1 Sub-bandgap filtering

The influence of sub-bandgap filtering is observed in figure (5.6) to push the maximum efficiency slightly higher and to promote larger cell thicknesses. This is to be expected. As the proportion of sub-bandgap photons is reduced, free-carrier absorption decreases, hence there is less of a penalty for thicker cells.

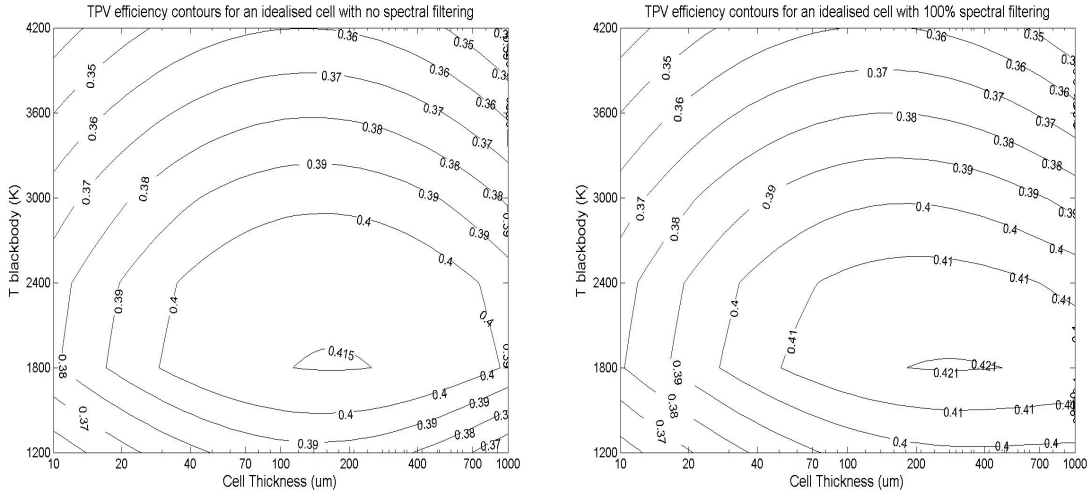

(a) **(b)**

Figure 5.6: (a) An idealised conventional cell with incident power normalised to $1\,\mathrm{W/cm^2}$, and no spectral filtering. **(b)** An idealised conventional cell with no incident sub-bandgap photons, removing the effects of free-carrier absorption. A slight shift towards higher cell thickness is observed, with a corresponding small increase in efficiency. The observed discontinuities at 1800 K and 2400 K are a result of the interval size of investigated blackbody temperatures.

As mentioned in section (5.2), for constant incident power densities, efficiency is observed to be only weakly dependent on cell thickness. For realistic TPV systems, incident power density would be optimised for each blackbody temperature and thickness, and an increase in efficiency for lower blackbody temperatures would be expected also.

From figure (5.6) it is observed that free-carrier absorption is a relatively small cause of efficiency decrease in thicker cells.

5.3.2 Above-bandgap filtering

Above bandgap ($E > 1.42\,\text{eV}$) spectral filtering returns high-energy photons to the emitter. Reducing the absorption of high-energy photons reduces blue-loss. For practical TPV systems this also leads to a reduction in heat load caused by photon thermalisation.

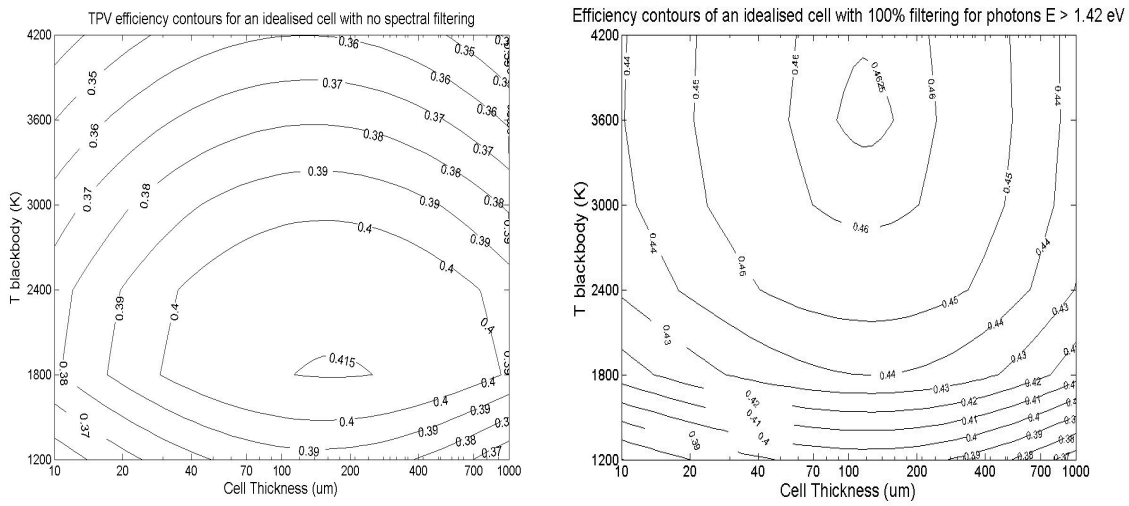

(a) **(b)**

Figure 5.7: (a) An idealised conventional cell with 50 % filtering above 1.42 eV. **(b)**The same cell with complete filtering of photons with energies above 1.42 eV. A marked increase in efficiency for higher blackbody temperatures is observed. A slight shift towards lower cell thicknesses is also observed.

As expected, a shift of maximum efficiency towards higher blackbody temperatures and thinner cells is observed in figure (5.7). The shift is relatively large for optimal blackbody temperature; increasing from ∼1800 K to ∼3600 K. Part of this shift is due to decreased blue-loss; with above-bandgap filtering higher temperatures are favourable where there are greater proportions of photons with $E_g < E < 1.42\,\text{eV}$. Part of this shift is also attributed to the decrease of transport loss with less short-circuit current density. For higher temperatures with less incident light and subsequently less current density, transport resistances are reduced.

Decreased transport resistance cannot be the reason for the shift of maximum efficiency to lower cell thicknesses. With above-bandgap filtering, optimal cell thickness would have to be *higher* to account for transport resistance. Maximum efficiency has increased by ∼5 %, and shifted to lower thicknesses from ∼190 μm to ∼110 μm. As a result of this work it is observed that blue-loss causes a significant reduction in efficiency for decreasing cell thickness.

5.3.3 Ideal spectral filtering

The ideal spectral filter in a perfect TPV system is that of de Vos' calculations presented in section (3.1): a monochromatic filter at the semiconductor bandgap energy [2].

In a less than ideal system, the optimal spectral filter must broaden to include higher proportions of above-bandgap photons. This section investigates filtering of both above and below bandgap photons, first at 50% filtering then subsequently at 100% filtering. This involves the reflection of 50 % of photons with energies less than the bandgap and greater than 1.42 eV, and subsequently complete reflection of all photons with E: $E < E_g$ and $E > 1.42\,\text{eV}$.

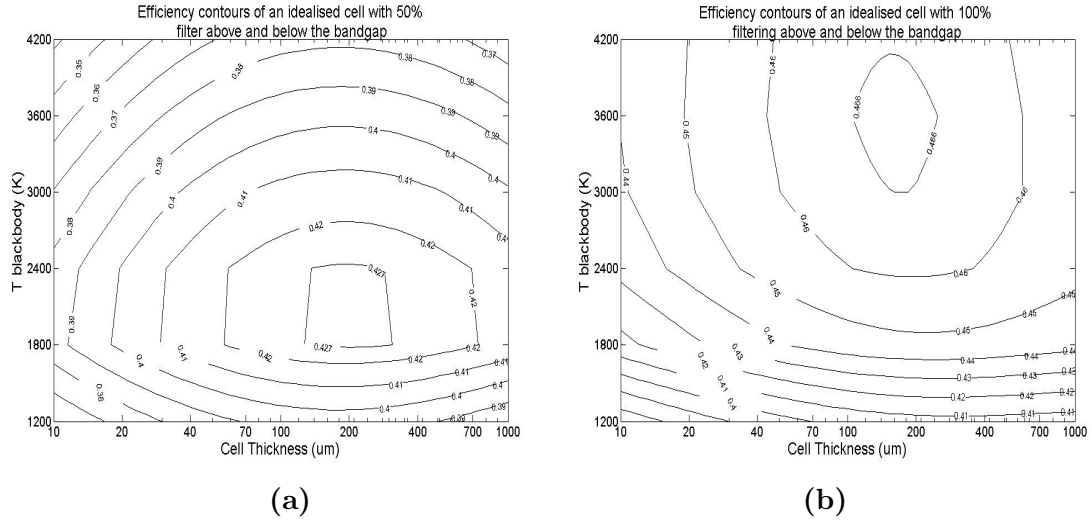

(a) **(b)**

Figure 5.8: **(a)**50 % above and below bandgap filtering for an idealised conventional cell with constant incident power density. **(b)**100 % above and below bandgap filtering of the same sysem. A shift towards higher temperatures is observed, and also a slight shift towards thin cells. The efficiency maximum is observed to be fairly broad across the range of cell thicknesses.

The resulting effect is a combination of the shifts in maximum efficiency observed in the previous two sections. From figure (5.8) it is observed that at constant incident power density, blue-loss and decreased transport resistance have stronger effect on efficiency than free-carrier absorption in the temperature direction. It is also observed that blue-loss has stronger effect than free-carrier absorption in cell thickness direction. That blue-loss limits efficiency at least as strongly as free-carrier absorption for thin cells is a key finding of this thesis.

Spectral effects are largely moderated when incident power density is optimised and resistive losses are observed to the main factor in determining optimal cell thickness. However, the initial expectation was that spectral considerations alone favour thin cells in TPV systems. This study shows that this is not the case.

5.4 Flat optical losses

This section examines the effect of flat, wavelength-independent optical losses on TPV system efficiencies. Sources for flat optical loss include the gaps between individual cells, bonding materials and the geometry of the TPV device. In a cylindrical system with a diameter to height ratio of 1:3 (for example, the cylindrical prototype TPV system in figure (2.7)), with cells covering only the side wall of the cylinder a flat optical loss of $\sim 15\,\%$ is already obtained.

The following is an examination of the *effect* of flat loss, to give an indication of the effect of TPV geometry on optimal cell thickness and blackbody temperature.

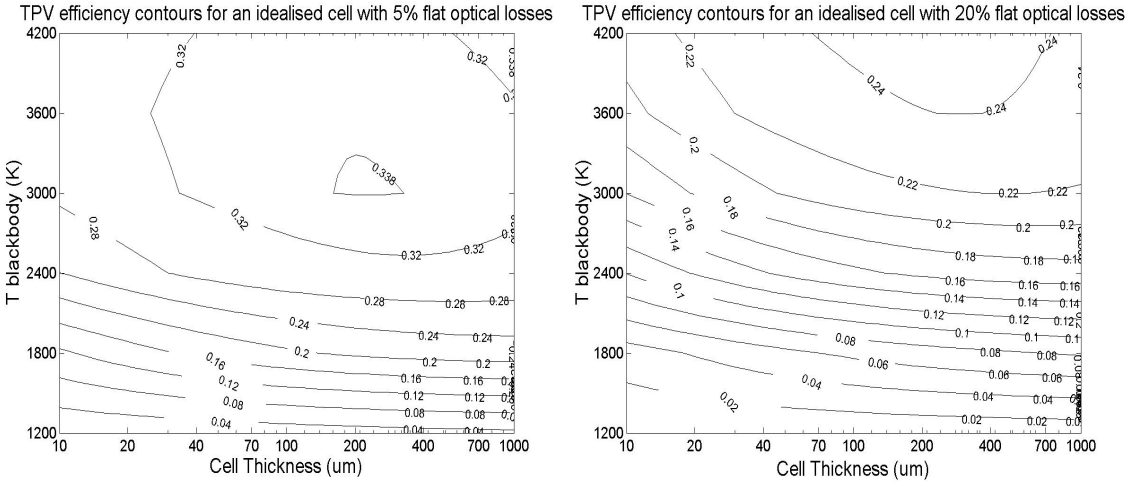

(a) **(b)**

Figure 5.9: (a)5 % flat optical losses for an idealised conventional cell with constant incident power density. (b)20 % flat losses for the same system. A significant reduction in efficiency and a shift towards higher blackbody temperatures is observed. The above cell was not modelled with any wavelength-dependent spectral filtering.

In agreement with expectations, we found that flat optical losses have a large impact on system efficiency. Both a large shift towards higher temperatures and a smaller shift towards higher cell thicknesses were observed. The shift towards higher temperatures is for the same reasons of blue-loss and decreased transport resistance as in the previous section. The small shift of optimum cell thickness is due to a balance of the factors of blue-loss shifting optimal thicknesses lower, and decreased transport resistance shifting optimal thicknesses higher.

5.4.1 Mirror reflectivity

The effect of mirror reflectivity on TPV systems was also examined. The analysis was for flat wavelength-independent mirror reflectivities of 95% and 90% followed by a simulation using the measured reflectivity data of the silver mirror used in the conventional and sliver analyses. Mirror reflectivity was found to have a similar effect on TPV efficiency as flat optical losses. This was expected since flat mirror reflectivity has an effect approximately equivalent to flat optical loss. The difference is that light has been able to pass once through the cell. The silver mirror was found to have an absorption that had similar effect

to a flat optical loss of ∼3 %; in agreement with its weighted reflectance value of 96.6 % (section (4.10)).

With incident power density optimised for each temperature and cell thickness (sections (5.7) and (5.8)) the effect of flat optical losses is to proportionally decrease efficiency for all temperatures and thicknesses. This is because incident power density will be increased to its previous optimum value to compensate for the flat optical loss.

5.5 Cell temperature

The final effect investigated for a cell under constant incident power density was cell temperature. As discussed in section (4.9), excellent heat-sinking of cells in a TPV systems is essential. This section examines the effect of cell temperature on an idealised TPV system.

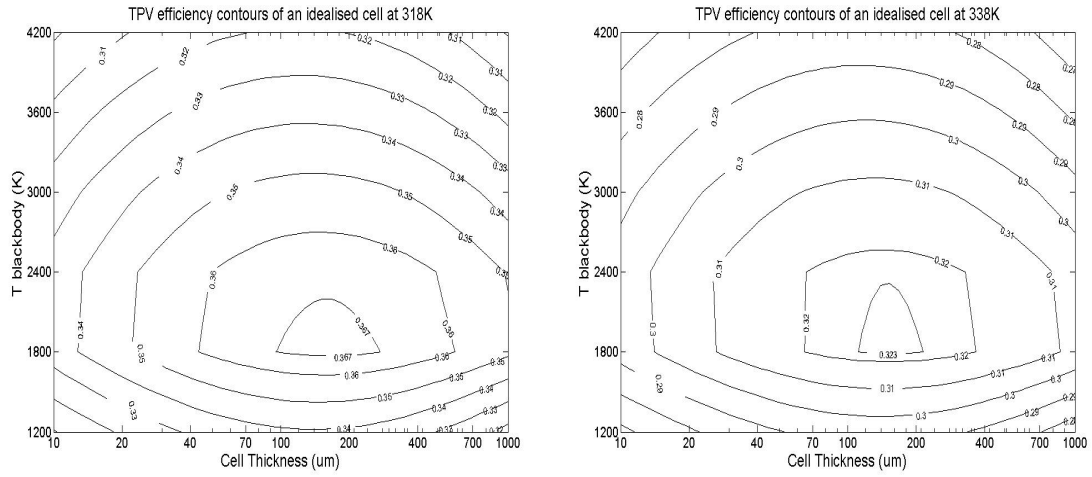

(a) **(b)**

Figure 5.10: **(a)**An idealised conventional cell at 318 K. **(b)**An idealised conventional cell at 338 K. The effect of increased cell temperature is observed to be a uniform decrease in efficiency over all thicknesses and temperatures

The effect of cell temperature is observed to decrease system efficiency fairly evenly over the range of blackbody temperatures and cell thicknesses. This is a result of the linear temperature coefficients of open-circuit voltage and fill factor discussed in section (4.7). The decrease is appreciable; for a cell temperature rise of $20°C$, maximum efficiency has dropped by more than 4% compared to the cell operating at $298K$. This is larger than the efficiency change over the whole range of examined cell thicknesses at $298K$. For a cell temperature rise of $40°C$ above room temperature, the decrease in efficiency is larger than the increase due to perfect spectral filtering of the idealised system.

Cell temperature is confirmed to be an important consideration of TPV systems, as observed in [29], [33] and [45].

5.6 Summary of individual TPV components

The modelling of an ideal cell at constant incident power density enabled an examination of the effects of individual TPV components on maximum efficiency.

The analysis of spectral filtering indicated that blue-loss limits TPV efficiency at least as strongly as free-carrier absorption. This is a key finding of this thesis. The initial expectation was that spectral considerations favour thin cells in TPV systems. This study shows that this is not the case.

Flat optical losses were observed to have a significant impact on TPV efficiency. This was as expected. Flat losses result in a proportional decrease in efficiency and shift optimal blackbody temperatures higher, due to blue-losses and decreased transport resistance. Mirror absorption has approximately the same effect as flat-optical losses, and was similarly observed to significantly decrease TPV efficiency.

Confirming earlier investigations of TPV systems [29, 33, 45], cell temperature was found to strongly influence efficiency, causing a uniform decrease in efficiency for all cell thicknesses and blackbody temperatures. The effect of cell temperature was observed to be of at least the same importance as spectral considerations.

Stemming from this work, practical recommendations to future TPV system designers are:

1) To ensure the optimisation of TPV geometry in order to minimise flat optical losses;
2) To ensure the highest quality available mirror is used, and;
3) To ensure cell cooling systems are optimised.

These are considered to be of equal importance as the optimisation of spectral filtering.

Further recommendations arise from the analysis of TPV cells in systems for which incident power density is optimised.

5.7 Conventional cells in TPV systems

Having examined the effect of individual components above, a conventional cell in a realistic TPV system was analyzed. This cell was modelled as an excellent back-contact cell with material properties as outlined in section (4.7). The cell had vertical transport losses, no lateral resistance losses, no optical flat losses and a rear surface weighted reflectance value of 0.3. The temperature of the cell was 318 K. Emitter thickness was 1.2 μm, sheet resistivity was 40 $\Omega/\square$ and IQE was set at 99 %. The MgF_2/ZnS double-layer antireflectance coating (section (4.11)) and optimal silver mirror (section (4.10)) were used. Each of these parameters were chosen to reflect an excellent, achievable, realistic cell.

Incident power density was optimised for each blackbody temperature and cell thickness. Optimisation entailed adjusting the dilution factor (section (4.2)) to obtain the maximum efficiency, the code for which is included in Appendix A. Physically, the optimisation of power density involves adjusting the distance between the cell and emitter surfaces, for each cell thickness and blackbody temperature, until the maximum efficiency at each point is found.

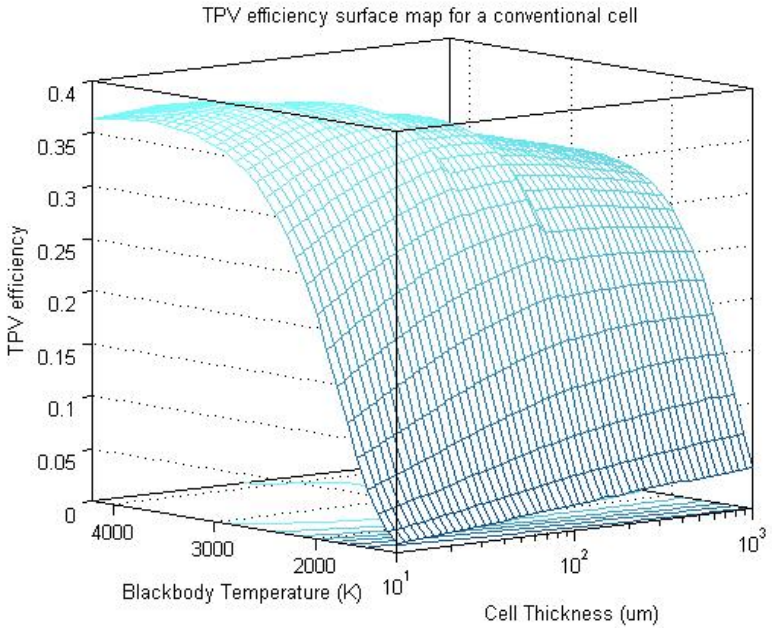

Figure 5.11: Conventional cell TPV efficiency surface. An efficiency maximum for low cell thicknesses and high blackbody temperatures is observed.

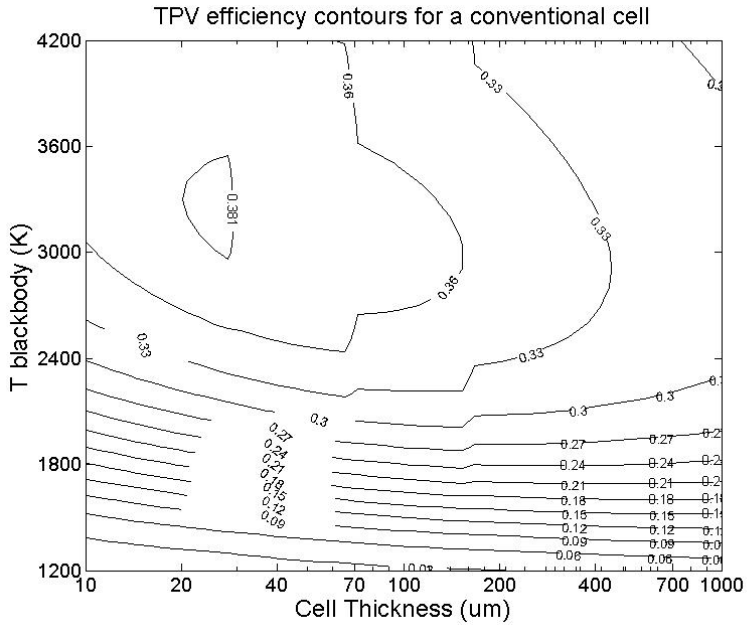

Figure 5.12: Observing the contours for the conventional cell, TPV efficiency is seen to be largely independent of thickness at low blackbody temperatures and optimised for low thickness at higher blackbody temperatures. This is a result of the optimisation of incident power density. The discontinuities observed at $\sim 30, 70$, and $160\,\mu$m are a result of adjusting bulk resistivities according to cell thickness to ensure high IQE (section (4.5)). An efficiency maximum of $(38 \pm 2)\,\%$ is observed, where the uncertainty is considered from the analysis presented in section (4.12).

Optimum TPV efficiency is observed in figures (5.11) and (5.12) to be for thin cells; $\sim 25\,\mu$m at a blackbody temperature of $\sim 3300\,$K. That the TPV efficiency is largely independent of cell thickness at lower temperatures is due to the relatively high bandgap of silicon. For low bandgap semiconductors, the efficiency structure of figure (5.12) would be shifted to lower temperatures. That the ideal blackbody temperature for silicon TPV cells is observed at $\sim 3300\,$K, indicates that silicon TPV cells are not likely to be feasible for current TPV systems, even with the consideration of reduced cost. An approximate absolute $10\,\%$ difference (28 - 38 %) is observed between the efficiencies at $2000\,$K and $3000\,$K. As outlined in section (5.10) silicon cells would have to operate with very high blackbody temperatures to compete with the performance with gallium antimonide cells. Cost advantages of silicon are expected to be offset by increased costs due to higher operating temperatures and the resulting need for very good systems materials and cooling systems. The efficiency decrease for blackbody temperatures T$>$ 3300 K is a result of blue-loss; the increase in the absorbed proportion of photons with $\epsilon \gg \epsilon_{bg}$. The structure observed in figure (5.12) having only slight decrease for higher temperatures indicates that for thin cells, blue loss is largely moderated through the optimisation of incident power density.

An examination of the power density optimisation is illustrated in figure (5.13).

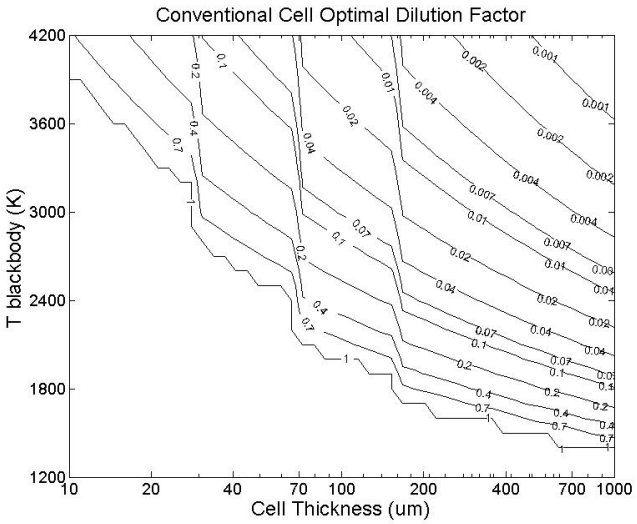

Figure 5.13: The optimal dilution factor for conventional cells. This factor controls the incident power density on the cells. Physically f is the ratio of surface areas of the emitter object and cell module (figure 4.1); a value of 1 indicates that optimal power density is obtained by having the cell directly adjacent to the radiating surface. As for figure (5.12) the discontinuities are a result of adjusting bulk resistivities according to cell thickness IQE (section 4.5).

For conventional cells it is observed that efficiency maxima are found for the highest J_{sc} possible (and hence higher V_{oc} and power output) before transport resistance losses start to dominate. This results in a dilution factor of 1 for low thicknesses and blackbody temperatures. Since the absorption of above-bandgap photons is low for thin cells and lower blackbody temperatures; it is optimal for the cells to collect as much light as possible. This is achieved by placing the TPV cells adjacent to the radiating surface, ie. a dilution factor of 1.

As temperature and cell thickness increase, the proportion of absorbed photons of $\epsilon > \epsilon_g$ and 'available' J_{sc} respectively increase. The optimal incident power density is then the level at which gains in efficiency through increased power output are balanced by resistance losses due to increased J_{sc}.

That the limiting factor of efficiency for thick cells is resistance losses and not free-carrier absorption, is illustrated in the following section (5.8) in which the efficiency maximum for sliver cells is for *high* thicknesses, due to decreased transport resistance.

The effect of incident power density optimisation on cell current density can be observed in figure (5.14), and the optimal value of J_{sc} for each cell thickness is illustrated in figure (5.15).

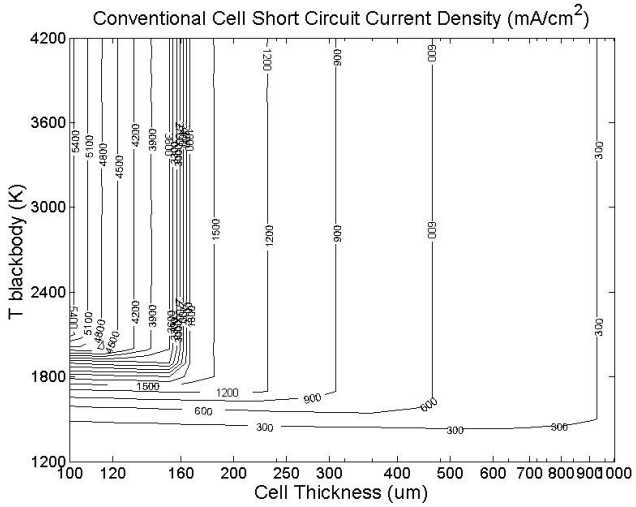

Figure 5.14: The vertical contour lines are the optimum J_{sc} values for each thickness. That they are vertical illustrates that optimum J_{sc} is dependent on cell thickness. This is observed in more detail in figure (5.15). High current densities greater than 5 A/cm^2 are observed for low cell thicknesses due to lower transport resistance losses. The sharp increase at 160 μm is due to the change of bulk resistivity at that thickness.

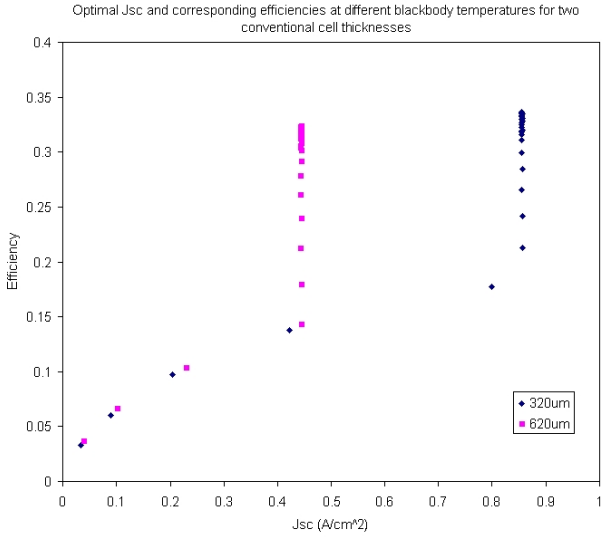

Figure 5.15: This figure illustrates the reason for the vertical contours of figure (5.14). For low temperatures and thicknesses, J_{sc} is limited by how close the cells can be to the emitter. As blackbody temperature and available photons with energy $\epsilon > \epsilon_{bg}$ increase, J_{sc} increases until the balance is found between increased output power density and increased resistive losses. This value of J_{sc} is then held for each thickness. Optimum Jsc is higher for thinner cells due to less vertical transport resistance losses through the cell.

In realistic TPV systems, the important factor is not solely the TPV efficiency: $\eta = E_{out}/E_{in}$. The magnitude of electrical power delivered by the system is an important consideration also. For instance, a TPV system may return 0.1 W of electrical power from 0.2 W of heat energy in - giving a TPV efficiency of 50 %. A more desirable performance would be from a system that returned 10 W of electrical power from 21 W of supplied heat energy. Due to the significant costs of TPV cells it is not practical to simply scale the area of cell modules. Achievable output power density is an important consideration for TPV cells.

As a result, we consider the power density contours of the TPV system in figure (5.16).

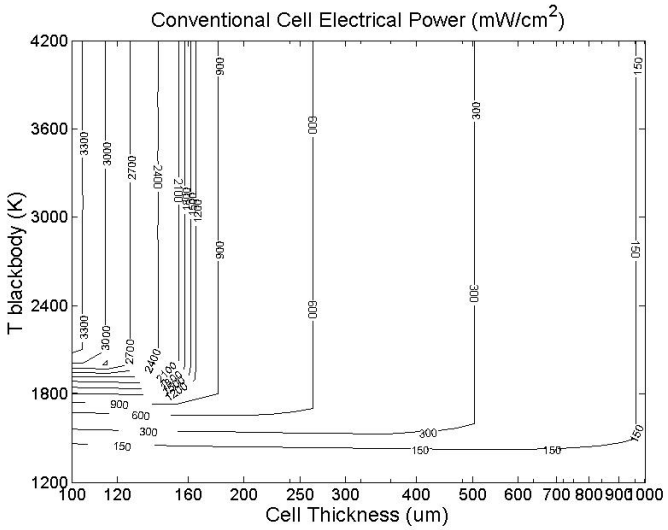

Figure 5.16: As a result of the J_{sc} contours of the conventional cell (figure (5.14)), electrical power density increases for thinner cells. High output power densities of $\sim$3 W/cm^2 are observed for thin cells.

These high electrical power densities are a result of the TPV geometry in which incident power density on the cell can be increased by placing the cells very close to the radiating surface. Photons not used by the cells are able to be reflected back to the emitter surface.

The reflection of photons back to the emitter is observed to be significant. At the maximum-efficiency conditions for conventional cells (thickness $\sim$25 μm and blackbody temperature $\sim$3300 K), approximately 60 % of the radiated spectrum power is returned to the emitter. The returned power is found to be greater than 40 % across the whole range of cell thicknesses and blackbody temperatures. This highlights a key feature of TPV systems that below bandgap radiation can be returned to the emitter, thus conserving its energy.

The results for conventional cells obtained by this study are in reasonable agreement with the work done by Swanson in 1978 who found the TPV efficiency maximum for idealised conventional silicon cells to be 42 % at 25 μm and 3000 K [14], compared to our observed maximum efficiency of (38$\pm$2) % at $\sim$25 μm and $\sim$3300 K. The difference between this project's TPV model and Swanson's calculations may be explained by the reflection of light from cell metal contacts, and by different absorption coefficients, choice of bulk resistivities, emitter sheet resistances and anti-reflection coating.

In both figures (5.16) and (5.14), the results have been presented for cell thicknesses greater than 100 μm. The reason for this is twofold. Firstly, the optimisation of incident power density for conventional cell thicknesses $< 100\,\mu$m led to very high values of J_{sc}

and electrical power density that remove the cell from the region of normal operation. At very high injection and J_{sc}, minority carrier lifetimes decrease, Auger recombination (a fundamental and avoidable loss mechanism detailed in [47]) becomes significant and the fill factor can no longer be calculated with equation (4.20). Conventional cells are limited to $100\,\mu$m also for the reason that this represents a practical lower limit for the manufacturing of back-contact cells; even for high-value applications such as thermophotovoltaics. $100\,\mu$m was also considered by Swanson to be the lower limit of practical cell thickness [14].

None the less, it is clear that for conventional cells in TPV systems, optimal cell thickness is as low as can be practically manufactured. TPV efficiency is at a maximum for thin cells. Electrical output power density, an equivalently important consideration for TPV systems, is also observed to be at a maximum for thin cells.

These results agree well with past findings, and formed the motivation for the study of sliver cells in TPV systems, whose method of fabrication readily allows for very thin cells.

5.8 Sliver cells in TPV systems

The final simulation was of a sliver cell in the TPV system. The cell had material parameters as outlined in section (4.5); double layer MgF_2/ZnS antireflective coating, silver back mirror, and 1 % flat optical losses due to the small area needed to join the slivers together. The cell was modelled at a constant 318 K, back surface reflectivity was set to 0.03. A minimum cell width of 300 μm was chosen, and the emitter region of the cell was set as 1.2 μm thick with a sheet resistance of 40 $\Omega/\square$. As for conventional cells, each of these sliver cell parameters were chosen to reflect an excellent, achievable, realistic cell.

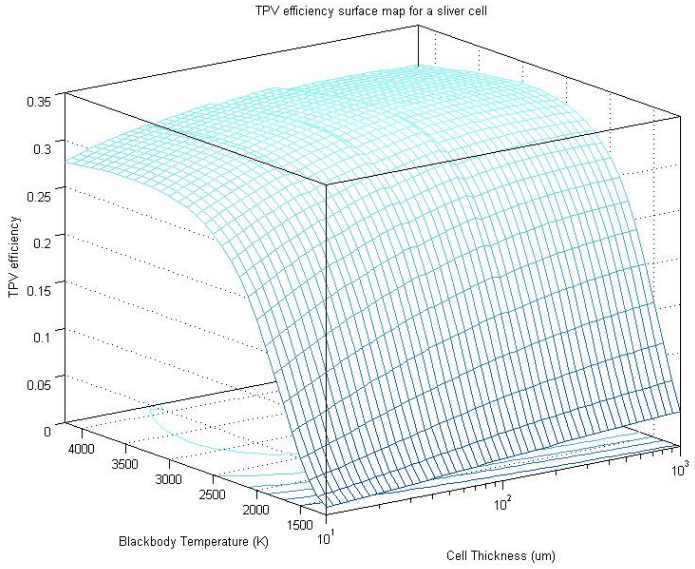

Figure 5.17: Sliver cell TPV efficiency surface. As for conventional cells, optimal performance is observed at high blackbody temperatures. In contrast with conventional cells, maximum efficiency is observed for *higher* cell thicknesses.

Similar to conventional cells, the maximum efficiency for sliver cells is observed at a high blackbody temperature of ∼3000 K, due to the relatively high bandgap of silicon.

TPV efficiency is observed to be largely independent of cell thickness at low blackbody temperatures. For higher blackbody temperatures, a small increase in efficiency is observed for *larger* cell thicknesses. This was contrary to the initial expectation that the thinness of slivers would provide increases in efficiency. This result due to the transport resistance structure of sliver cells.

As outlined previously, sliver cells have their metal contacts at the edges of the cell. Transport losses are hence not vertically through the cell, but laterally between the contacts. The broad maximum in figure (5.18), with only ∼3 % change in efficiency across the whole range of cell thicknesses, is due to the main limiting factor of sliver cell performance being *emitter* resistance.

Emitter resistance depends on the *square* of cell width.

$$P_{sliver\ emitter\ loss}\% = \frac{R_{\square} W^2 J_{mp}}{3 V_{mp}}$$

With cells fixed at a minimum width of 300 μm and emitter thickness held at 1.2 μm (to avoid excessive surface recombination losses), emitter losses do not change with overall cell thickness.

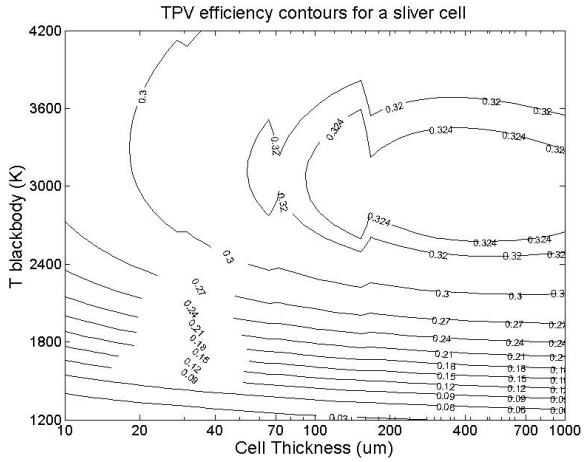

Figure 5.18: The maximum efficiency for sliver cells is observed to be (32 ± 2)Åpproximately 85 % of the maximum efficiency of conventional cells. TPV efficiency is observed to be largely independent of cell thickness at low blackbody temperatures, similarly to conventional cells. As blackbody temperatures increase, efficiencies are found to be at a maximum for *higher* thicknesses. This is a result of the cell-contact geometry of sliver cells.

In contrast to conventional cells, bulk resistance losses *decrease* with cell thickness (equation (4.23))

$$P_{sliver\,bulk\,loss}\% = \frac{\rho W^2 J_{mp}}{3HV_{mp}}$$

The efficiency maximum for thick cells is a result of decreasing resistive power losses for thicker sliver cells.

A key observation of thesis is made from figure (5.18). That the efficiency maximum for sliver cells is at high cell thicknessess indicates that resistive losses have stronger effect than free-carrier absorption at high illumination intensities. This was contrary to our initial expectation. It is from the original investigation of this thesis into the different resistance geometry of sliver cells that the effects can clearly be separated.

Sliver cell relative maximum efficiencies were found to be $\sim 85\,\%$ of those achieved by conventional cells. The corresponding difference was larger than the uncertainty range of the model (section (4.12)).

From these observation it is clear that sliver cells do not have an advantage over conventional cells in TPV systems. While sliver cell thicknesses can readily be less than $100\,\mu$m, sliver *widths* are limited (by assumption) to $300\,\mu$m, sliver transport resistive losses depend on the square of the cell width and as a result sliver cells will be limited to current and output power densities significantly lower than corresponding thin conventional cells. The examination of the optimisation of incident power density is presented in figure (5.19). This effect of transport losses on sliver current and electrical power densities is illustrated in figure (5.20)

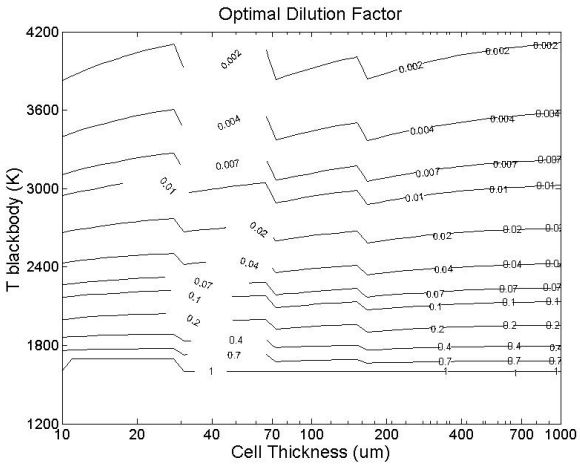

Figure 5.19: The structure of optimal dilution reflects the importance of resistance losses. For low temperatures; the highest possible concentration is optimal. For increasing temperature and photons with energies $\epsilon > \epsilon_{bg}$, incident power density is reduced to maintain optimum J_{sc}. The effect of reduced bulk resistance loss due to increasing thickness is observed with the rising slope of the dilution factor in the direction of increasing thickness. The discontinuities at $30, 70$, and $160\,\mu m$ are where bulk resistivities are adjusted for cell thickness and IQE.

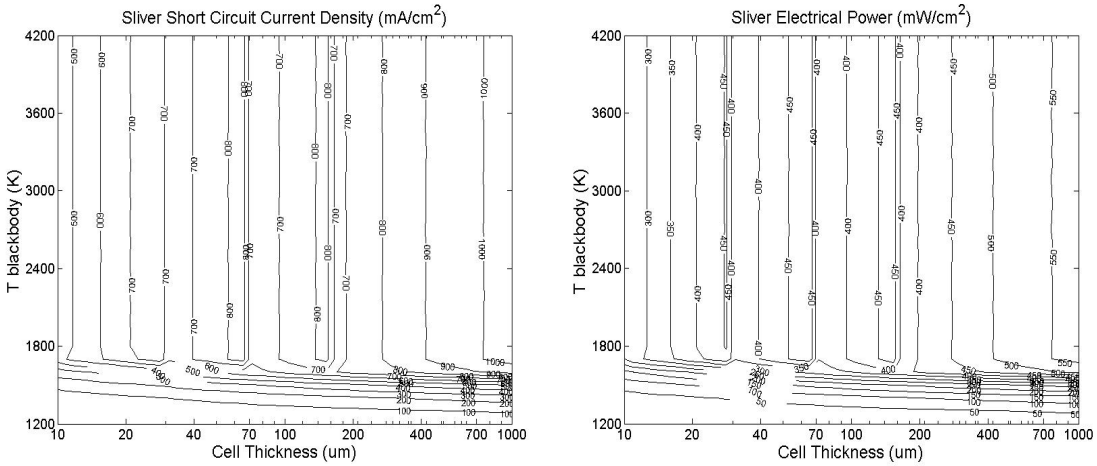

(a) **(b)**

Figure 5.20: As a result of tranport resistances optimal J_{sc} and electrical power density contours are both fairly uniform across cell thickness, slightly increasing for higher thicknesses. The vertical contours are due to the optimal values of J_{sc} for each thickness, as discussed for conventional cells. The main observation from these figures is that maximum values of J_{sc} and electrical power density; $(1000 \pm 50)\,\mathrm{mA/cm^2}$ and $(600 \pm 30)\,\mathrm{mW/cm^2}$ respectively, are lower than those for conventional cells by a factor of five.

While the maximum efficiency of sliver cells is only ∼85 % of the maximum efficiency of conventional cells, in figure (5.20) it is observed that achievable electrical output densities are a factor of 5 times lower. This ia strong disadvantage for sliver cells in TPV systems.

Transport through the emitter is observed to be the main limiting resistance loss for sliver cells. To decrease this loss, the emitter sheet resistance can be lowered. However, as examined in section (4.5.2), decreasing emitter sheet resistance leads to a reduction in internal quantum efficiency. The optimum value was observed to be $40\,\Omega/\square$; below this, decreasing IQE offsets the gain accrued through lowered resistance.

It is observed that the inherent geometry of sliver cells limits their potential efficiency in TPV systems. For sliver geometries to be advantageous in TPV systems the *width* of the sliver cells must decrease to values below the normal lower limit ($300\,\mu$m). Due to the fabrication process of sliver cells this means starting with a thin wafer ($< 300\,\mu$m).

This may be feasible; reducing sliver widths by a factor of two (from 300 to $150\,\mu$m) allows for a factor of 4 increase in illumination intensity and output power density for the same percentage of resistive loss. The disadvantage of this approach is the consideration of handling large numbers of thin, narrow sliver cells. The investigation into the feasibility of narrow sliver cells is presented as the subject of a possible future study.

The sliver technique of fabricating cells from within the wafer bulk allows practical cell thicknesses of the order of tens of micrometers; approximately 10 times thinner than conventional cell thicknesses. Sliver cells are well suited to TPV systems with the one exception of having metal contacts at the edges of the cell. Were it possible to manufacture cells using the sliver technique of fabrication, except having the contacts at the top and bottom surfaces of the sliver instead of at the edges, the resulting cells would be exceptionally suited for use in TPV systems.

Such cells have not yet been manufactured; for sliver solar cells under normal sunlight illumination, edges on the side of the cell are a distinct advantage [15, 16], and contacts on the top and bottom would detract significantly from performance.

For thin cells in TPV systems, top and bottom contacts resulting in vertical carrier transport are a distinct advantage, slightly offset by practical considerations outlined in section (5.9). There are two possible ways in which vertical carrier transport can be incorporated with sliver technology. The first is to fabricate sliver cells while the slivers are still in the wafer as outlined by Franklin (2006) [16], except with metallisation of the top and bottom surfaces of the sliver instead of at the edges (figure (2.5)). Both top and bottom contacts are necessary for sliver cells due to their bifacial nature. Fabrication of these contacts could be achieved by laser etching of the top and bottom surfaces of the cell, and subsequent diffusion and metal evaporation to form the contacts. Laser etching is routinely undertaken in various steps of sliver fabrication [27]. The difference for the fabrication of TPV cells is that the laser would need to etch along the entire surface of the cell while it is still in the wafer. A possible future research direction is to investigate whether this may be achieved with a wide laser beam.

A second possibility is to fabricate metal contacts into the top and bottom of the cell *after* the slivers have been removed from the wafer. The advantage of this method is that contact metallisation could proceed as for conventional cells. The disadvantage is the consideration of handling and processing large numbers of thin slivers. This may be found to be reasonable for high-value application such as high-efficiency TPV cells for military or deep-space power generation.

5.9 Extra TPV considerations

Alongside cell efficiency and electrical power output considerations for TPV systems, are the more practical design issues of heat-sinking, non-uniform radiation of the emitter, and cell module circuitry.

As observed in section (5.5), cell temperature is an important consideration for TPV systems. That sliver cells have their contacts on the side of the cell is an advantage for heat sinking; thermally conducting material with an integrated mirror can be bonded directly to the back-surface of the cell allowing for excellent heat conduction [16]. For back contact cells, heat-sinking is more difficult. The back surface must accommodate the mirror, the electrical contacts, and the electrical conductors while maintaining a low risk of short circuits between n and p contacts. Very good heat sinking has been achieved with conventional cells built for concentrated sunlight systems. For TPV systems with the inclusion of a back-surface mirror, heat sinking for conventional cells is much harder.

Another consideration for TPV systems is the non-uniform radiation of the TPV emitter. This poses problems for the circuit design of cells in a TPV system. Cell shading can lead to reverse breakdown and malfunction the cell module - just as for cells under solar radiation. The narrow width of sliver cells allow for cells to be easily connected in sub-modules that reduce the risk of reverse cell breakdown. In addition, narrow width allows sliver cells to be connected in series to rapidly build voltage. While the output power of sliver and conventional modules will be the same, the sliver module will be operating at higher voltage, instead of higher current, this is illustrated in figure (5.21). Since resistance losses vary with the square of the current $P=I^2R$, external circuit resistances are significantly higher for conventional modules than sliver cell modules.

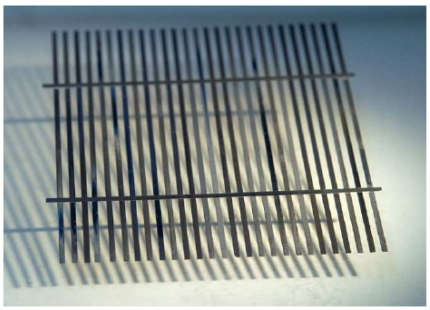

Figure 5.21: A photo of a sliver cell submodule for use in normal solar panels. Voltage is built across the 27 individual slivers, to give an output voltage of $\sim 27\times 0.6\,\mathrm{V}$. A conventional cell with the same surface area as the surface area of the above slivers, would operate with a high current, but remain at $\sim 0.6\,\mathrm{V}$. [16]

For optimal TPV cells operating at high current densities, metal contacts that connect the cell to the external circuit need to be sufficiently thick to minimise ohmic resistance losses. When the computational model was constructed, the high level of current density at which TPV systems can operate was not initially expected, and the contact area for conventional back-contact cells was assumed to be negligible. In practice, for high current densities, back-contact metal contact surface area would increase to be at least equivalent with the area of sliver cell contact, if not larger. While metal contacts will reflect significant amounts of the incident light, increased contact area will increase parasitic absorption. For high current densities, sliver cells with contacts at the edges of the cell offer an advantage in terms of decreased optical losses resulting from light incident on the metal contacts.

The above considerations favour sliver cell geometries for practical TPV systems. How-

ever, for the current limits of sliver cell dimensions examined in this study, they are not considered significant enough to compensate the increased efficiency and 5-times-higher output power of conventional cell geometries.

5.10 TPV cell summary and extrapolation to GaSb

Within the range of parameters examined, it was observed that sliver cells do not offer a clear advantage over well designed conventional cells in TPV systems.

That sliver cells have efficiency maxima at high emitter temperatures indicates that resistive losses have stronger effect in TPV systems than free-carrier absorption at high illumination intensities. This was contrary to our initial expectation. It is from the original investigation of this thesis into the different resistance geometry of sliver cells that the effects can clearly be separated.

The model indicated that high illumination intensities are desirable in order to take advantage of higher open-circuit voltages, to be achieved by placing the cells close to the emitter. Sliver cell performance in TPV systems was found to be limited by horizontal carrier transport resistance through the width of sliver cells. While sliver cell thicknesses can be manufactured to be less than 100 μm, sliver *widths* in this study were limited to 300 μm. Since sliver transport resistive losses depend on the square of the cell width, sliver cells were limited to current densities and output power densities significantly lower than corresponding thin conventional cells.

Sliver cell maximum efficiencies $(32 \pm 2), \%$ were found to be $\sim 85\,\%$ of the maximum efficiency achieved by conventional cells $(38 \pm 2)\,\%$. Sliver cell maximum output power densities $(600 \pm 30)\,\mathrm{mW/cm^2}$were lower than those for conventional cells $(3300 \pm 100)\,\mathrm{mW/cm^2}$)by a factor of five.

Practical considerations of heat-sinking, submodule resistances, and metal contact area at high incident power densities were found to favour sliver cells. For current limits of sliver cell dimensions examined in this study, these advantages are not expected to outweigh the limited power density of sliver cells.

Optimal cells for thermophotovoltaic systems were found to be thin back-contact cells with spectral filtering that reflected high energy photons back to the emitter. The primary advantage for thin cells in TPV systems was observed to be a result of decreased resistive losses and not spectral considerations.

Optimal blackbody temperatures for silicon TPV cells were found to be $\sim$3300 K. Though TPV efficiencies of $\sim$30 % were observed for the upper limit of realistic TPV temperatures of $\sim$2400 K, gallium antimonide (GaSb) cells are expected to have these efficiencies at TPV temperatures of $\sim$1300 K. While the focus of this study is not of economic considerations, cost advantages of silicon due to availability and mass manufacturing are expected to be offset by increased costs due to higher emitter operating temperatures and the resulting need for very good systems materials and cooling systems.

In extrapolating the findings of this study to GaSb, three properties were important to consider: 1) the bandgap energy, 2) the absorption coefficient structure and 3) the resistivity of the semiconductor material.

GaSb has a bandgap of 0.72 eV [42, 18] with an absorption structure similar to silicon; high absorption for high-energy photons, decreasing exponentially below the bandgap illustrated in figure (4.8).

Because of the similar absorption structure, an approximate interpretation between silicon and GaSb absorption can be made with blackbody temperature. With the energy of the photon of maximum emission (E_{max}) proportional to blackbody temperature from Wien's Law: $E_{max} = \frac{hc}{\beta}T$, with β Wien's constant, we can predict to first order that the

behaviour of GaSb will correspond to the behaviour of silicon for blackbody temperatures ∼900 K less than those for silicon.

The behaviour of GaSb due to the resistivity of cell materials is harder to correlate. Indeed, the main reason for not investigating GaSb in detail was the lack of available data on material resistivites and corresponding minority carrier diffusion lengths for doped GaSb materials. However, we can use as an example a real GaSb cell to gain a comparison of resistivities. One such cell, examined by Stollwerck *et al* [37], had a Te-doped n-type 300 μm thick bulk with doping density of $5 \times 10^{17}\,\mathrm{cm}^{-3}$ and resistivity of 0.01 Ω.cm and Zn-doped p-type 0.55 μm thick emitter of density $1 \times 10^{20}\,\mathrm{cm}^{-3}$ with sheet resistance 13 Ω/□.

These are lower than for silicon. Lower resistance losses for GaSb would lead to higher optimum power densities than for silicon. In addition, the maximum efficiency point would be expected to shift towards higher J_{sc}.

Most importantly, although the values of maximum efficiency will change, the *structural* properties are not expected to change between silicon and gallium antimonide. The optimal gallium antimonide cell for thermophotovoltaic systems is expected to be similar to that for silicon; a thin back-contact conventional cell with spectral filtering that reflects high energy photons back to the emitter.

The key findings of this study are expected to be the same for gallium antimonide cells. That is, resistive losses have stronger effect than free-carrier absorption at high illumination intensities. Blue-losses are an equally important spectral consideration as free-carrier absorption. And the primary advantage for thin cells in TPV systems is a result of decreased resistive losses and not lower free-carrier absorption.

Conclusions and Future Research

6.1 Conclusions

This thesis has presented an original analysis of silicon sliver cells in thermophotovoltaic systems. A computational model was constructed that allowed simulation of photovoltaic cells in realistic TPV conditions. The model was validated through comparison with the device modelling program PC1D under non-TPV conditions. Excellent agreement was observed.

Within the range of parameters examined, it was found that sliver cells do not offer a clear advantage over well designed conventional cells in TPV systems. The model indicated that high illumination intensities are desirable in order to take advantage of higher open-circuit voltages, to be achieved by placing cells close to the emitter. Sliver cell output power densities at these illumination intensities were observed to be strongly limited by horizontal transport resistance. This is due to sliver contacts being at the edges of the cell, resulting in resistive power losses that vary as the square of cell width. Minimum sliver cell widths in this study were limited to $\sim 300\,\mu m$. As a result, series resistance losses for sliver cells were found to be significantly higher than for thin conventional cells with vertical carrier transport.

Within the assumptions of the model, sliver cell maximum efficiencies $(32 \pm 2)\,\%$ were found to be $\sim 85\,\%$ of the maximum efficiency achieved by conventional cells $(38 \pm 2)\,\%$. Sliver cell maximum output power densities $(600 \pm 30)\,\mathrm{mW/cm^2}$ were lower than those for conventional cells $(3300 \pm 100)\,\mathrm{mW/cm^2}$ by a factor of five.

Practical considerations of heat-sinking, submodule resistances, and metal contact area at high incident power densities were found to favour sliver cell geometries. For the current limits of sliver cell dimensions examined in this study, these advantages are not expected to outweigh the limited power density of sliver cells.

Optimal cells for thermophotovoltaic systems were found to be thin back-contact cells with spectral filtering that reflected high energy photons back to the emitter. The primary advantage for thin cells in TPV systems was observed to be a result of decreased resistive losses and not spectral considerations. This was contrary to initial expectation. It is from the original investigation of this thesis into the different resistance geometry of sliver cells that these effects can clearly be separated.

Blue-losses due to the absorption of high-energy photons (with subsequent thermalisation loss of the excess energy) were found to be a significant spectral loss component for thin cells. Free-carrier absorption, which was expected to be substantial for thick cells, was found to be of lesser relative importance.

Modelled cells were composed of silicon. Silicon cells were found to perform well at emitter temperatures that are above the current range of feasibility for TPV systems. The cost advantages of silicon to other semiconductor materials are expected to be offset by

increased costs due to higher emitter operating temperatures and the resulting need for very good emitter materials and cooling systems.

Modelling results were considered for gallium antimonide cells. Due to the similar absorption coefficient structure, GaSb cells are expected to perform similarly to Si cells, at temperatures ∼900 K below those for silicon.

The key findings of this study are expected to be the same for GaSb cells. That is, resistive losses have stronger effect than free-carrier absorption at high illumination intensities. Blue-losses are an equally important spectral consideration as free-carrier absorption. And the primary advantage for thin cells in TPV systems is a result of decreased resistive losses and not lower free-carrier absorption.

The optimal gallium antimonide cell for thermophotovoltaic systems is expected to be similar to that for silicon; a thin back-contact conventional cell with spectral filtering that reflects high energy photons back to the emitter.

6.2 Future research directions

Future research directions have been presented in various sections of this thesis. They are summarised for three areas; firstly, recommendations are made for the design of future TPV systems, secondly, potential fabrication processes for the manufacturing of optimal thermophotovoltaic cells are outlined, and finally, the properties of future whole-system thermophotovoltaic models are discussed.

From the analysis of an idealised cell under constant incident power density in section (5.3), three key practical recommendations for future TPV designers were made:

1) To ensure the optimisation of TPV geometry in order to minimise flat optical losses;
2) To ensure the highest quality available mirror is used, and;
3) To ensure cell cooling systems are optimised.

These are considered to be of equal importance as the optimisation of spectral filtering. In addition to TPV design considerations, further research awaits the optimisation of photovoltaic cells for use in TPV systems.

It is observed that the inherent geometry of sliver cells limits their potential efficiency in TPV systems. For sliver cell performance in TPV systems to be comparable to conventional cells, the *width* of the sliver cells must decrease to values below the normal lower limit (300 μm). Due to the fabrication process of sliver cells this means starting with a wafer with thickness less than $< 300\,\mu$m.

This may be feasible; reducing sliver widths by a factor of two (from 300 to 150 μm) allows for a factor of 4 increase in illumination intensity and output power density for the same percentage of resistive loss. This is a consequence of sliver transport resistive losses depending on the square of cell width. While the performance of 150 mum wide sliver cells would still be lower than that for well-designed thin conventional cells, maintaining sliver cell contact geometry allows for the practical sliver cell advantages of heat-sinking and cell-module circuitry to remain. The disadvantage of this approach is the consideration of handling large numbers of thin, narrow sliver cells. The investigation into the feasibility of narrow sliver cells is presented as a subject of possible future study.

The results of section (5.7) indicate that the optimal cell in TPV systems is a thin ($< 100\,\mu$m) back-contact cell. The sliver technique of fabricating cells from within the wafer bulk allows cell thicknesses that are in the tens of micrometers. Sliver cells are well suited to TPV systems with the one exception of having metal contacts at the edges of the cell.

As presented in section (5.8), there are two possible ways in which sliver technology could be used to fabricate thin cells with vertical carrier transport. The first is to fabricate

sliver cells while the slivers are still in the wafer as outlined by Franklin (2006) [16], except with metallisation of the top and bottom surfaces of the sliver instead of at the edges (figure (2.5)). Fabrication of these contacts could be achieved by laser etching of the top and bottom surfaces of the cell, and subsequent diffusion and metal evaporation to form the contacts.

A second possibility is to fabricate metal contacts into the top and bottom of the cell *after* the slivers have been removed from the wafer. The advantage of this method is that contact metallisation could proceed as for conventional cells. The disadvantage is the consideration of handling and processing large numbers of thin slivers. This may be found to be reasonable for high-value application such as high-efficiency TPV cells for military or deep-space power generation.

For the optimisation of photovoltaic cells in TPV systems, a different future direction of research is the investigation of cell texturing for TPV cells. From the modelling results of this thesis, it was observed that the advantage of thin cells in TPV systems is due to decreased resistive losses, and not lower levels of free-carrier absorption. Cell surface texturing has the effect of coupling more light into the cell and increasing the optical path length of photons, without increasing physical cell thickness and transport resistances. The disadvantage of texturing is that the recycling of photons back to the emitter is decreased. The investigation of the balance of these processes is presented as a future research direction.

The optimisation of thermophotovoltaic systems requires accurate and detailed modelling. This is required both of detailed cell device parameters, and of TPV systems as a whole.

The results of this study indicate that high illumination intensities are desirable for TPV systems in order to achieve high output power densities. To be able to perform at high output power densities, TPV cell material parameters must be optimised to reduce resistive losses but still provide high internal quantum efficiencies. An important area of further study for the TPV field is to find the lowest resistivity values for gallium antimonide cells for which this is possible. It is after these resistivities are found that whole systems modelling can accurately optimise blackbody temperatures and the components of spectral filtering.

Due to the relative youth of feasible TPV technology, and possibly also due to the competitive and commercially driven nature of the field, a comprehensive model of TPV systems has not yet been established. This is in contrast to solar photovoltaics where a number of device models are available for use. The future development of a model that could accurately simulate each stage of TPV energy conversion from the generation of source heat to cell cooling mechanisms, would be extremely useful for the field. An area of required research for TPV systems is the development of a model that uses accurate simulation methods for photon ray-tracing through the system, coupled with a detailed device modelling program which would calculate cell performance characteristics. A suitable model could potentially be developed through a combination of the RACER-X Monte Carlo ray-tracing program outlined by Aschaber *et al* [45], and the DESSIS semiconductor device modelling software used by Franklin [16].

Appendices

A.1 Nonlinear semiconductor equations

The full set of coupled non-linear semiconductor equations that device modelling programs use to calculate photovoltaic cell performance are given by [16]:

$$\begin{aligned} \epsilon \nabla \overrightarrow{E} &= q(p - n + N_d^+ - N_a^-) \\ \nabla \overrightarrow{J_n} &= q(R - G) + q\frac{\partial n}{\partial t} \\ \nabla \overrightarrow{J_p} &= -q(R - G) - q\frac{\partial n}{\partial t} \\ \overrightarrow{J_n} &= q\mu_n \overrightarrow{E} + qD_n \nabla n \\ \overrightarrow{J_p} &= q\mu_p \overrightarrow{E} - qD_p \nabla p \end{aligned} \tag{A.1}$$

These equations are the Poisson charge neutrality equation, the electron and hole continuity equations, and the electron and hole transport equations respectively.

Electron density and hole density are denoted by n and p. $\overrightarrow{E}$ is the electric field and $\overrightarrow{J_n}$ and $\overrightarrow{J_p}$ are the electron and hole current densities respectively. N_d^+ and N_a^- are the donor and receptor doping densities. R and G are the recombination and generation rates, and μ_n, D_n, μ_p and D_p are the electron and hole mobilities and diffusivities respectively.

A.2 Dilution factor optimisation code

Sub Generate Cont Data

```
'optimise for diln factor
 'first optimise with a rough grid
    'select the grain with q, q neq 1
     q = 100

   MaxEff1 = 0
   MaxDiln1 = 0
   MaxEff2 = 0
   MaxDiln2 = 0

   For k = 1 To q
     DilF1(k, 1) = 10 ^ ((4 * k / (q - 1)) + ((-4 * q) / (q - 1)))
```

```
    Range("fdilution").Select
    Selection = DilF1(k, 1)

      'make sure Power Loss is <10%
      'choose for either Conventional or Sliver resistance
      'schemes with plosstransport or plossbulk

       'PLossCheck = 0
        PLossBulkCheck = 0
        Sheets("Thermo Model").Select
        'Range("PlossTransport").Select
        Range("PlossBulk").Select
        'PLossCheck = Selection
        PLossBulkCheck = Selection
       MaxPLoss = 0.1
      'If MaxPLoss > (PLossCheck) Then
      If MaxPLoss > (PLossBulkCheck) Then

    Range("SysEff").Select
    DilF1(k, 2) = Selection
    If DilF1(k, 2) > MaxEff1 Then
      MaxEff1 = DilF1(k, 2)
      MaxDiln1 = DilF1(k, 1)
        'make sure the parameters for the
        'fine study are for 1<k<q,
        If MaxEff1 = DilF1(1, 2) Then
         MaxDiln1m1 = DilF1(1, 1)
         MaxDiln1p1 = DilF1(2, 1)
        End If
        If MaxEff1 = DilF1(q, 2) Then
         MaxDiln1m1 = DilF1(q - 1, 1)
         MaxDiln1p1 = DilF1(q, 1)
        End If
        If MaxEff1 <> DilF1(1, 2) Then
        If MaxEff1 <> DilF1(q, 2) Then
          MaxDiln1m1 = DilF1(k - 1, 1)
          MaxDiln1p1 = DilF1(k + 1, 1)
     End If
     End If
    End If
    End If
  Next k

'If the maximum is at the limit
'then skip the fine study
If MaxEff1 = DilF1(q, 2) Then
  MaxEff2 = MaxEff1
  MaxDiln2 = MaxDiln1
End If
```

```
  If MaxEff1 = DilF1(1, 2) Then
    MaxEff2 = MaxEff1
    MaxDiln2 = MaxDiln1
  End If



  If MaxEff1 <> DilF1(q, 2) Then
  If MaxEff1 <> DilF1(1, 2) Then
  'next optimise with a fine grid
    MaxEff2 = 0
    MaxDiln2 = 0

    'choose the grain with n, n neq 1
     n = 100

    For m = 1 To n
      DilF2(m, 1) = (((MaxDiln1p1 - MaxDiln1m1) / (n - 1)) * m) + ((n * MaxDiln1m1
      Range("fdilution").Select
      Selection = DilF2(m, 1)

      Range("fdilution").Select
      Selection = DilF2(m, 1)
      Range("SysEff").Select
      DilF2(m, 2) = Selection
        If DilF2(m, 2) > MaxEff2 Then
         MaxEff2 = DilF2(m, 2)
         MaxDiln2 = DilF2(m, 1)
       End If
    Next m
  End If
  End If

'put in optimal diln factor
    Range("fdilution").Select
    Selection = MaxDiln2
    MD(i, j, 10) = MaxDiln2"
```

Glossary

Blue-losses The efficiency loss process in TPV systems resulting from the absorption of photons with energies much higher than the semiconductor bandgap.

DESSIS A semiconductor device modelling program capable of simulating carrier transport in 2 and 3 dimensions.

FF_0 Ideal fill factor. The fill factor of a photovoltaic cell with ideality factor of 1, without internal series or shunt resistance.

FF The final fill factor incorporating internal series and shunt resistances of a photovoltaic cell.

Fill factor The ratio of maximum output power density of the photovoltaic cell to the product of short-circuit current density and open-circuit voltage.

Free-carrier absorption The absorption of photons with energies below the semiconductor bandgap. Free-carrier absorption does not contribute to electrical power.

Ideality factor The factor that determines which recombination processes dominate the performance of a solar cell

J_0 Reverse saturation current density.

J_{sc} Short-circuit current density.

M*ü*ser engine A direct heat-conversion engine with a heat dilution factor.

Open-circuit voltage The voltage at which no current flows through a diode.

PC1D A one-dimensional semiconductor device modelling program developed at Sandia National Laboratories.

Reverse saturation current density The recombination current density for an ideal diode without illumination.

Sheet resistance A measure of resistivity per unit of cross sectional area, with units of $\Omega/\square$. Used to express the resistivity of photovoltaic emitter regions.

Short-circuit current density The current density of a photovoltaic device under illumination when the contacts are shorted.

Thermophotovoltaics The approach of using photovoltaic cells to generate electricity from the radiated spectrum of adjacent hot objects.

V_{oc} Open-circuit voltage.

Bibliography

[1] W. Shockley and H. Queisser, "Detailed balance limit of efficiency of p-n junction solar cells," *Journal Applied Physics*, vol. 32, pp. 510–519, March 1961.

[2] A. deVos, *Endoreversible Thermodynamics of Solar Energy Conversion*. Oxford: Oxford University Press, 1992.

[3] N. Harder and P. Wurfel, "Theoretical limits of thermophotovoltaic solar energy conversion," *Semiconductor Sci. Technol.*, vol. 18, pp. S151–S157, 2003.

[4] USA Department of Energy *Website* Accessed May 2007,

`http://www.energy.gov/news/4503.htm`

[5] V. Andreev *et al.*, "Solar thermophotovoltaic system with high temperature tungsten emitter," pp. 671–674, Photovoltaic Specialitsts Conference, 31st IEEE, 2005.

[6] K. Stone *et al.*, "Operation and component testing of a solar thermophotovoltaic powersystem," pp. 1421–1424, PV Specialists Conference, Twenty-Fifth IEEE, 1996.

[7] K. Stone *et al.*, "Testing and modeling of a solar thermophotovoltaic power system," vol. 358, pp. 199–212, 2nd NREL Conference on TPV Generation of Electricity, 1996.

[8] V. Andreev *et al.*, "Thermophotovoltaic converters with solar powered high temperature emitters," 20th European Photovoltaic Solar Energy Conference, 2005.

[9] T. Coutts, "A review of progress in thermophotovoltaic generation of electricity," *Renewable and Sustainable Energy Reviews*, vol. 3, pp. 77–184, 1999.

[10] L. fraas et al, "Commercial GaSb cell and circuit development for the Midnight Sun tpv stove," vol. 460, pp. 480–487, AIP Conf. Proc. Fourth NREL conference on TPV generation of electricity, 1999.

[11] D. Wilt *et al.*, "Thermophotovoltaics for space power applications," Seventh World Conference on TPV Generation of Electricity, 2007.

[12] G. Guazzoni and S. Matthews, "A retrospective of four decades of military interest in thermophotovoltaics," vol. 738, pp. 3–12, 6th Conference on TPV Generation of Electricity, AIP, 2004.

[13] L. Fraas *et al.*, "Thermophotovoltaic system configurations and spectral control," *Semicond. Sci. Technol*, vol. 18, no. 5, pp. S165–S173, 2003.

[14] R. M. Swanson, "Silicon photovoltaic cells in thermophotovoltaic energy conversion," *International Electron Devices Meeting*, vol. 24, pp. 70–73, 1978.

[15] A. Blakers, K. Weber, *et al.*, "Sliver cells - a complete photovoltaic solution," IEEE 4th World PV Energy Conversion Conference, May 2006.

[16] E. Franklin, *PhD Thesis: Sliver Solar Cells and Concentrator Sliver Cells.* July 2006.

[17] D. Clugston and P. Basore, "Pc1d version 5: 32-bit solar modelling on personal computers," pp. 207–210, PV Specialists Conference 26th IEEE, 1997.

[18] S. Adachi, *Optical Constants of Crystalline and Amorphous Semiconductors.* Massachusetts: Kluwer Academic Publishers, 1999.

[19] C. Kittel, *Introduction to Solid State Physics, 8th Edition.* U.S.A: John Wiley & Sons, 2005.

[20] S. Sze, *Semiconductor Devices, Physics and Technology, 2nd Edition.* U.S.A: John Wiley & Sons, 2002.

[21] A. Blakers *et al.*, "22.8 % silicon solar cell," *Applied Physics Letters*, vol. 55, no. 13, pp. 1363–1365, 1989.

[22] M. Green *et al.*, "Characterisation of 23 % efficient solar cells," *IEEE Transactions on Electron Devices*, vol. 37, no. 2, pp. 331–336, 1990.

[23] M. Green, *Third Generation Photovoltaics - Advanced Solar Energy Conversion.* Berlin: Springer, 2003.

[24] M. Green *et al.*, "Solar cell efficiency tables (version 26)," *Progress. Photovolt. Res. Appl*, vol. 14, no. 5, pp. 455–61, 2006.

[25] M. Green and D. Jordan, "Technology and economics of three advanced silicon solar cells," *Progress in Photovoltaics: Research and Applications*, vol. 6, no. 3, pp. 169–180, 1998.

[26] R. Sinton *et al.*, "Developments in module ready Si backside-contact solar cells," pp. 302–306, PV Specialists Conference 21st IEEE, 1990.

[27] A. Blakers, *Personal communications.* Australian National University, 2006/07.

[28] R. Nelson, "A brief history of thermophotovoltaic development," *Semiconductor Sci. Technol.*, vol. 18, pp. S141–S143, 2003.

[29] T. Coutts *et al.*, "An overview of the fifth conference on thermophotovoltaic generation of electricity," *Semicond. Sci. Technol*, vol. 18, no. 5, pp. S144–S150, 2003.

[30] R. Mahorter *et al.*, "Thermophotovoltaic system testing," *Semicond. Sci. Technol*, vol. 18, no. 5, pp. S232–S238, 2003.

[31] V. Andreev *et al.*, "Tandem gasb/ingaassb thermophotovoltaic cells," pp. 935–938, Photovoltaic Specialists Conference, Twenty-Sixth IEEE, 1997.

[32] T. Coutts, "An overview of thermophotovoltaic generation of electricity," *Solar Energy Materials and Solar Cells*, vol. 66, pp. 443–452, 2001.

[33] D. Martin and C. Algora, "Key issues for an accurate modelling of GaSb tpv converters," (Rome, Italy), pp. 442–451, Fifth conference on TPV Generation of Electricity, 2002.

[34] D. Burger and R. Mueller, "Thermophotovoltaic system paramteric modelling," pp. 1863 – 1866, Twenty-fourth IEEE, PV Specialists Conference, 1994.

[35] A. El-Husseini and J. L. Gray, "Numerical modelling of thermophotovoltaic cells and systems," pp. 959–962, Photovoltaic Specialists Conference, Twenty-Sixth IEEE, 1997.

[36] A. Bett and O. V. Sulima, "GaSb photovoltaic cells for applications in tpv generators," *Semiconductor Science and Technology*, vol. 18, no. 5, pp. S184–S190, 2003.

[37] G. Stollwerck *et al.*, "Characterization and simulation of GaSb device-related properties," *IEEE Transactions on electron devices*, vol. 47, no. 2, pp. 448–456, 2000.

[38] C. Algora and D. Martin, "Modelling GaSb thermophotovoltaic converters under real conditions," (Munich, Germany), 17th European Photovoltaic Solar Energy Conference, 2001.

[39] C. Algora and D. Martin, "Modelling and manufacturing GaSb tpv converters," (Rome, Italy), Fifth Conference on TPV Generation of Electricity, 2002.

[40] M. Zenker *et al.*, "Efficiency and power density potential of combustion-driven thermophotovoltaic systems using GaSb photovoltaic cells," *IEEE Transactions on Electron Devices*, vol. 48, no. 2, pp. 367–375, 2001.

[41] O. Sulima and A. Bett, "Fabrication and simulation of GaSb thermophotovoltaic cells," *Solar Energy Materials and Solar Cells*, vol. 66, pp. 533–540, 2001.

[42] D. Martin and C. Algora, "Temperature-dependent GaSb material parameters for reliable thermophotovoltaic cell modelling," *Semicond. Sci. Technol*, vol. 19, pp. 1040–1052, 2004.

[43] E. Cashwell and C. Everett, *Monte Carlo for random walk problems*. London: Pergamon Press, 1959.

[44] C. Moglestue, *Monte Carlo Simulation of Semiconductor Devices*. London: Chapman & Hall, 1993.

[45] J. Aschaber *et al.*, "Realistic modelling of tpv systems," *Semicond. Sci. Technol.*, 2003.

[46] R. Deckman and Yablonovitch, "Maximum statistical increase of optical absorption in textured semiconductor films," *Optics Letters*, vol. 8, no. 9, pp. 491–493, 1983.

[47] M. Green, *Solar Cells*. New Jersey: Prentice-Hall, 1986.

[48] M. Green, *High Efficiency Silicon Solar Cells*. Switzerland: Trans-Tech, 1987.

[49] L. Ferguson and L. Fraas, "Theoretical study of GaSb PV cells efficiency as a function of temperature," *Solar Energy Materials and Solar Cells*, vol. 31, pp. 11–18, 1994.

[50] E. Radziemska, "The effect of temperature on the power drop in crystalline silicon solar cells," *Renewable Energy*, vol. 28, pp. 1–12, 2002.

[51] V. Everett *et al.*, "Characterisation of the thermal response of sliver cells and wafers," (Paris), 19th European PV Solar Energy Conference, 2004.

[52] Spectrolab *Website*, Accessed December 2006

`http://www.spectrolab.com/DataSheets/K6700B/k6700b.pdf`

[53] National Astronomical Observatory of Japan *Website*, Accessed October 2006,

`http://www.naoj.org/Observing/Telescope/Parameters/Reflectivity}`

[54] O. S. Heavens, *Optical Properties of Thin Solid Films*. London: Butterworths Scientific Publications, 1955.

[55] D. Boufhas *et al.*, *Design and simulation of antireflection coating systems for optoelectronic devices: Application to Silicon Solar Cells*, vol. 52. 1998.

[56] R. R. et al, "Validation and error estimation of computational models," *Reliability Engineering and System Safety*, vol. 91, pp. 1390–1397, 2006.